Title

Experimental determination of calcite solubility in H2O-KCl-NaCl-LiCl solutions at 700 °C and 8 kbar

Permalink

https://escholarship.org/uc/item/9db113sv

Author

Eguchi, James Hiro

Publication Date

2014

Peer reviewed|Thesis/dissertation

UNIVERSITY OF CALIFORNIA

Los Angeles

Experimental determination of calcite solubility in H_2O-KCl-NaCl-LiCl solutions

at 700 °C and 8 kbar

A thesis submitted in satisfaction

of the requirements for the degree Master of Science

in Geology

by

James Hiro Eguchi

2014

ABSTRACT OF THE THESIS

Experimental determination of calcite solubility in H_2O-KCl-NaCl-LiCl solutions

at 700 °C and 8 kbar

by

James Hiro Eguchi

Master of Science in Geology

University of California, Los Angeles, 2014

Professor Craig E. Manning, Chair

Understanding the interactions between calcite and aqueous solutions is important when studying the deep carbon cycle. The present study investigates the solubility of calcite in salt-H_2O fluids at 700 °C and 8 kbar. The investigated salts included NaCl, KCl, LiCl, and CsCl. All experiments were conducted in a piston cylinder apparatus. The results show that calcite solubility increases with increasing concentration of any individual salt. The data were successfully fit to simple functions of the square of salt mole fraction. At a given salt concentration, the solubility enhancement increases with decreasing salt cation size. Experiments in the fluids with mixtures of multiples of salts were used to derive simple relations that can be used to predict calcite solubility in a wide range of salt solutions at the studied conditions. The results provide a basis for extending this approach to different pressures, temperatures, and salt compositions.

The thesis of James Hiro Eguchi is approved.

Edwin A. Schauble

Edward D. Young

Craig E., Manning, Committee Chair

University of California, Los Angeles

2014

TABLE OF CONTENTS

LIST OF TABLES

LIST OF FIGURES

ACKNOWLEDGMENTS

1. INTRODUCTION

Carbon plays a vital role in controlling the habitability of the planet's surface. Carbon dioxide levels in Earth's atmosphere have a large effect on surface temperatures and acidity of the oceans (Royal Society and U.S. National Academy of Sciences, 2014). Therefore, it is important to understand Earth's carbon reservoirs and the fluxes between these reservoirs. Great effort has been devoted to understanding how carbon is cycled on Earth's surface, but the deep carbon cycle has received relatively less attention until recently. Subduction of sediments and oceanic lithosphere transport several hundred Mt/yr of CO_2 into the Earth's interior (Plank and Langmuir 1998; Alt and Teagle, 1999; Ague and Nicolescu 2014). The deep carbon cycle controls Earth's climate on short to long timescales; at geologic timescales, subduction has the potential to transport all surface carbon to Earth's interiors (Dasgupta and Hirschmann, 2010). The fact that surface carbon persists shows that carbon is continuously cycled between Earth's interior and surface via subduction and volcanism (Dasgupta and Hirschmann, 2010; Dasgupta 2013).

The calcium carbonate ($CaCO_3$) minerals calcite and aragonite are the primary reservoir for oxidized carbon in the continental crust and upper mantle, and are the dominant carriers of carbon into the Earth's interior (e.g., Dasgupta and Hirschmann, 2010). Therefore, understanding the stability of calcium carbonate minerals under conditions relevant to Earth's interior is crucial to understanding the deep carbon cycle. Kerrick and Connolly (2001) showed that carbonates do not undergo metamorphic devolatilization in all but the hottest subduction zones. The stability of carbonates in subduction zones suggests that large amounts of carbon may be transported to the lower mantle (Kerrick and Connolly, 2001; Dasgupta and Hirschmann, 2010). However,

significant amounts of carbon are released via arc volcanism which shows that carbon is

somehow being released from subducted carbonates in subduction zones.

The mechanisms for releasing carbon from the subducting slab to the overlying mantle

wedge are poorly understood (Dasgupta and Hirschmann, 2010; Frezzotti et al., 2011). Possible

mechanisms for releasing carbon from the subducting slab are partial melting of carbonated

lithologies, modification of phase equilibria by H_2O, melting of sediment diapirs, and dissolution

of carbonates by an aqueous phase (Kerrick and Connolly, 2001; Newton and Manning 2002;

Caciagli and Manning, 2003; Dasgupta and Hirschmann, 2010; Marschall and Schumacher,

2012; Duncan and Dasgupta, 2013). As described below, a variety of natural examples support

the idea that dissolution of calcium carbonate by aqueous solutions plays a major role in the

transport and redistribution of carbon in Earth's crust and upper mantle.

1.1. Natural evidence for calcium carbonate dissolution in subduction zones

Recent studies have provided natural evidence of carbon mobilization by calcite

dissolution in subduction zones (Frezzoti et al., 2011; Bouilhol and Burg, 2012; Ague and

Nicolescu, 2014). Diamonds from ultra-high pressure rocks in the Italian western Alps have

fluid inclusions containing dissolved carbonate species as well as carbonate daughter minerals,

suggesting that carbonate dissolution is an important mechanism for releasing carbon from

subducting slabs (Frezzotti et al., 2011). Bouilhol and Burg (2012) studied calcite-olivine-

bearing veins in mantle rocks of Kohistan Paleo-Island Arc located in Northern Pakistan. Their

observations suggest that fluids released during slab dehydration may dissolve subducted

carbonates and transport them to the overlying mantle wedge (Bouilhol and Burg, 2012). Ague

and Nicolescu (2014) studied marbles from an exhumed ancient subduction zone on the Greek

islands of Syros and Tinos. Observation of the marbles showed that there were fluid conduits which were active during subduction. Analysis showed that as you approached the fluid conduits the abundance of calcium carbonate decreased, suggesting carbonate dissolution and transport (60-90% of CO_2 released from rocks). Ague and Nicolescu (2014) concluded that their observations suggest that dissolution of calcium carbonate minerals can release large amounts of the C from subducted slabs.

1.2. Natural evidence for calcium carbonate dissolution in crustal metamorphic terranes

The flux of carbon into the Earth at subduction zones is larger than the flux of carbon released from Earth's interior at arc volcanoes (Dasgupta and Hirschmann, 2010). This suggests that carbon is being transported deep into the mantle and stored there for long periods. Another possible explanation for the imbalance of carbon flux in to and out of Earth's interior is that aqueous fluids dissolve calcium carbonate from subducted lithologies and precipitate carbonates in the crust as the fluids move towards Earth's surface (Caciagli and Manning, 2003; Newton and Manning 2002). Manning and Ingebritsen (1999) suggested that the Earth may be permeable to mass transport by fluid flow to the base of the continental crust. Newton and Manning (2002) and Caciagli and Manning (2003) showed that at crustal conditions calcite becomes less soluble with decreasing pressures and temperatures, therefore as calcium carbonate rich fluids migrate through the permeable crust towards the surface the fluids will precipitate calcium carbonate, storing C in the crust.

Widespread calcite-bearing veins in Earth's crust provide natural evidence which demonstrates that crustal fluids are capable of dissolving and redistributing large amounts of calcium carbonate in the Earth's crust (Newton and Manning, 2002; Caciagli and Manning,

2003). In some medium- and high-grade metamorphic terranes, there is pervasive and vein-controlled carbonate metasomatism, sometimes replacing up to 20% of the country rock with carbonate, again demonstrating the large capacity of crustal fluids to transport calcium carbonate (Newton and Manning, 2002). Newton and Manning (2002) called these terranes carbonate megashear zones, which can be found in places such as the post-Hercynian South Tien Shan fault zone (Baratov et al., 1984), the Late Proterozoic Attur Valley of Tamil Nadu, India (Wickham et al., 1994), the Mid-Proterozoic Mary Kathleen Fold belt of Queensland, Australia (Oliver et al., 1993), and the Mid-Proterozoic Bamble Shear Belt of southern Norway (Dahlgren et al., 1993). Fluid inclusion analysis in some of these terranes showed that the fluids in some of these rocks were highly saline (Newton and Manning, 2002). Intrusions of gabbro, syenite, and carbonatite in some these terranes suggest a mantle origin for the metasomatizing fluids (Newton and Manning, 2002). These metamorphic terranes provide strong evidence supporting the large capacity of crustal fluids to dissolve and redistribute carbon in Earth's crust.

The fact that fluid inclusion analysis shows that many of these fluids were highly saline is important because Newton and Manning (2002) showed that calcite solubility increases with increasing NaCl concentration. There is now abundant evidence for highly saline fluids in metamorphic terranes (e.g., Newton et al., 1998; Newton and Manning, 2010; Manning and Aranovich, in press). Many fluid inclusion studies have reported the occurrence of salt daughter crystals in fluid inclusions (Xiao et al., 2001; Van den Berg and Huizenga, 2001; Nehring et al., 2009), which means that have X_{NaCl} must have exceeded 0.1 in these fluids (Manning and Aranovich, in press). The widespread occurrence of highly saline brines, coupled with the ability of saline brines to transport large amounts of dissolved $CaCO_3$ makes understanding calcite solubility in saline fluids important when studying the deep carbon cycle.

1.3. Previous work

Considering the evidence for carbon mobilization by dissolution in aqueous fluids, it is important to understand the interactions between calcite and aqueous solutions at high pressure and temperature. Previous authors have conducted experimental studies on calcite solubility in pure H_2O and aqueous NaCl solutions at high pressures and temperatures. Caciagli and Manning (2003) studied calcite solubility in pure H_2O at 6-16 kbar and 500-800 °C. They found that at high pressures and temperatures calcite solubility increases with increasing pressure and temperature. Newton and Manning (2002) studied calcite solubility in aqueous NaCl solutions at 600-900 °C at 10 kbar and 6-14 kbar at 700 °C. They found that in aqueous solutions containing NaCl, similar to pure H_2O, calcite solubility increases with increasing pressure and temperature. They also found that calcite solubility increased with increasing salt concentration up to near-saturation of NaCl.

1.4. Aims of study

The previous studies have focused on calcite solubility in pure H_2O and NaCl solutions. However, in natural systems, solutions rarely consist of only a single solute; natural solutions are almost always complex solutions, containing various different solutes. The present study was conducted to complement previous studies by Newton and Manning (2002) and Caciagli and Manning (2003) by focusing on how fluid composition affects calcite solubility. This study aims to investigate how different alkali halides such as KCl and LiCl affect calcite solubility at high pressures and temperatures. In order to better constrain calcite solubility in complex geologic

fluids this study also seeks to investigate how calcite solubility is affected when multiple salts are mixed in solution.

2. METHODS

2.1. Starting Materials

Experiments were designed to determine the solubility of calcite in aqueous solutions containing NaCl, KCl, LiCl, CsCl and their mixtures at high temperatures and pressures. Each experiment contained distilled and deionized ~18 MΩ cm^3/cm H$_2$O, salt (either a mixture of salts or a single salt), and pure natural calcite. Salts used in experiments were CsCl (Fisher Scientific, lot no 905414A, Certified reagent), KCl (Mallinckrodt, lot no. khlm, ACS reagent), NaCl (Fisher scientific, lot no 064062, ACS reagent), and LiCl (Fisher Scientific, lot no 921557, Certified reagent). The calcite was from Rodeo, Durango, Mexico, with 0.07 wt % FeO as the most significant impurity (Caciagli, 2001; Newton & Manning 2002). Individual inclusion-free calcite rhombs weighing 0.5-3.5 mg were smoothed using a diamond file, and then polished using 150 grit sandpaper.

2.2. Capsule Assembly

Experiments were performed using a double-capsule technique (Manning and Boettcher, 1994; Newton and Manning 2002). Inner capsules were cut to 7.5 mm length from platinum tubes (2 mm OD). One end of the capsule was crimped shut and the sharp corners were clipped and burnished to prevent puncturing of the outer capsule. A polished calcite crystal was weighed then placed inside the inner Pt capsule. The open end of the inner Pt capsule was crimped shut,

taking care not to damage the calcite crystal. The inner capsule was then punctured twice to allow penetration of the aqueous salt solution from the outer Pt capsule. Any extra platinum was then cut off and sharp corners were clipped and burnished, and the inner Pt capsule was weighed a final time.

The outer Pt capsule was cut to a length of 18 mm from a Pt tube (3.5 mm OD), and annealed using a Bunsen burner. One end of the capsule was then crimped and welded shut by graphite arc welding. After weighing, the inner Pt capsule was placed in the outer Pt capsule. Each time a new ingredient was added to the outer capsule, the capsule was weighed to get the mass of the added component by mass difference. After all salts were added, H_2O was added in amounts equal to or less than the desired mole fraction for the experiment. If H_2O was in excess of the target value, it was allowed to evaporate until the desired quantity was reached. Once all starting materials were added to the outer Pt capsule, the open end of the capsule was crimped shut taking care not to squeeze out any liquid. The end of the capsule was then welded shut. After welding, the capsule was reweighed to assure that significant amounts of liquid were not lost. If a significant amount of liquid was lost, the capsule was discarded; otherwise the capsule was placed in a 110 °C furnace for 15 minutes and reweighed as a final check on the integrity of the weld.

The variably hygroscopic nature of the alkali chlorides required special drying procedures. Salts were placed in a 300 °C furnace to drive off H_2O prior to loading. Extra measures were required for LiCl. After adding LiCl, the capsule was placed in a 300 °C furnace for 5 minutes to drive off absorbed H_2O. The capsule was weighed 45, 60, 90, and 120 seconds after removal from the furnace. The mass gained due to absorption of water depended linearly on time. Therefore to obtain the weight before absorption of water, weight was extrapolated to

time 0 using the weight measurements at 45, 60, 90, and 120 seconds. The water gain due to absorption was negligibly small relative to the bulk H_2O. It was therefore ignored in all calculations of salt mole fraction and solubility.

The masses of the starting calcite crystal and inner Pt capsule were determined on a Mettler Toledo ultramicrobalance with $1\sigma = 0.2$ μg. The masses of the outer Pt capsule and all materials were made on a Mettler M3 microbalance with $1\sigma = 2$ μg. Weighing uncertainties were determined by repeated weighings of a standard of known mass.

2.3. Experimental Apparatus and Set-up

All experiments were conducted in a 2.54 cm diameter end-loaded piston cylinder apparatus. Experiments were run in furnace assemblies which consisted of a NaCl pressure medium and graphite resistance heater (Bohlen 1984; Manning and Boettcher 1994).

Completed capsules were loaded into a furnace assembly with the long axis of the capsule perpendicular to the long axis of the assembly to minimize the vertical temperature gradient in the furnace (Manning and Boettcher 1994). A thin Pt sheet was placed on top of the capsule to prevent piercing of the capsule by the thermocouple during the run.

All experiments were conducted at 700 °C and 8 kbar. Temperature was monitored and controlled using Type S Pt-$Pt_{90}Rh_{10}$ thermocouples, with an uncertainty of ± 3 °C. Experiments used the piston-out technique, in which the apparatus was first pressurized to ~6 kbar, then heated. Thermal expansion typically brought the sample to the target pressure of 8 kbar with no additional pumping on the piston. At final run conditions the NaCl cells are frictionless, and require no pressure correction (Bohlen 1984; Manning and Boettcher 1994; Caciagli and Manning 2003;). Thermal expansion continued for about 3-6 hours, so pressure was bled to

8

maintain 8 kbar until apparatus reached thermal equilibrium. Pressure was held to within ±150 bars throughout the duration of the experiment.

All experiments were held at 700 °C, 8 kbar, for at least 4 hours (see below), then quenched by cutting power. Temperatures dropped rapidly to <100 °C in <1 min.

2.4. Solubility Determination

The quenched capsule was retrieved from the furnace assembly, soaked in distilled water for 5-10 minutes to dissolve any adhering NaCl, and dried at 110 °C. After drying, the capsule was weighed to ensure that no water was lost during the run. To assess whether solution was lost during the experiment, the capsule was punctured and placed in a 110 and 300 °C furnace to drive off all water. If LiCl was used in the experiment, the method discussed above was used to correct for hygroscopic behavior. The dry capsule was then reweighed. The mass difference between the full and dried capsule corresponds to the water out (Tables 1 and 2), and provides a check on fluid retention during an experiment.

The outer Pt capsule was then cut open with a razor blade, taking care not to damage the inner capsule. The outer capsule contained precipitated salts, and quenched skeletal calcite crystals which were collected and examined under a binocular microscope. The inner Pt capsule was then retrieved and inspected for any damage. If the inner Pt capsule had been damaged and appeared to have lost any Pt it was discarded.

The inner capsule was placed in a beaker of distilled water which was then stirred and heated. The capsule was then dried and weighed. This process was repeated until the inner capsule came to a constant mass, which signaled that all salts had been removed, leaving behind only insoluble calcite.

9

Calcite dissolves congruently in H_2O and H_2O-salt solutions (Newton and Manning, 2002; Caciagli and Manning, 2003; see below), so the weight change of a crystal during an experiment yields a direct measurement of solubility. However, increasing total salt concentration raises the possibility that the calcite crystal will break into pieces that make direct weighing challenging. This can be circumvented by determining the weight change of the inner capsule itself, provided that all dissolved calcite precipitated in the outer capsule upon quenching:

$$m_{CaCO_3} = \frac{1000(w_{ic}^i - w_{ic}^f)}{100.078 \, w_{H_2O}} \qquad (1)$$

where m_{CaCO_3} is concentration of $CaCO_3$ in solution in units of molality, w_{ic}^i and w_{ic}^f are the initial and final masses of the inner Pt capsules respectively, 100.078 is the molecular weight of $CaCO_3$, and w_{H_2O} is the mass of water present in the experiment (all values in mg).

If dissolved calcite precipitated in the inner capsule during quenching, the solubility determined by Eq. (1) only gives a minimum value. The accuracy of solubility determined this way was therefore checked in selected experiments by directly weighing calcite crystals where they could be recovered. To do this, the inner capsule was opened with a razor blade in a fashion similar to the outer capsule. The inner capsule contained undissolved calcite and small amounts of quenched skeletal calcite which could be distinguished based on texture under a binocular microscope. If the undissolved calcite crystal was unbroken or broken into just a few fragments they were separated from the quench crystals, then retrieved and weighed to give a maximum calcite solubility measurement via:

$$m_{CaCO_3} = \frac{1000(w_{cc}^i - w_{cc}^f)}{100.078\ w_{H_2O}} \quad\quad\quad (2)$$

where w_{cc}^i and w_{cc}^f are the initial and final masses of the calcite crystal respectively, in

milligrams. This solubility measurement is treated as a maximum, because it is possible that

some undissolved fragments of the calcite crystal were unnoticed and therefore unweighed. After

solubility measurements were made contents of the inner capsule were collected for textural

analysis on a Tescan Vega 3 scanning electron microscope (SEM).

2.5. Salt concentration notation

In the following discussion, the investigated range of salt identities and mixtures requires

several alternate ways of portraying salt concentrations. The total salt mole fraction, $X_{total\ salt}$, in a

solution of any number of salts is defined as:

$$X_{total\ salt} \equiv \frac{\sum_i\ n_i}{\sum_i\ n_i + n_{H_2O}} \qu\quad\quad (3)$$

where n is the number of moles of the subscripted species in the aqueous solution. The mole

fraction of a particular salt i in a solution with any number of salts is:

$$X_i \equiv \frac{n_i}{\sum_i\ n_i + n_{H_2O}} \qu\quad\quad (4)$$

For two-salt solutions, the molar ratio of salt i relative to the second salt, regardless of

$X_{total\ salt}$, is:

$$N_i \equiv \frac{n_i}{\sum_{i=1}^{i=2} n_i} \tag{5}$$

For three-salt solutions, the molar ratio of i relative to the other salts is:

$$\eta_i \equiv \frac{n_i}{\sum_{i=1}^{i=3} n_i} \tag{6}$$

3. RESULTS

Calcite solubility was determined at 700 °C and 8 kbar, in a range of salt solutions. Results are given in Tables 1 and 2. Experimental results were assessed by examining run-product textures and evaluating solubility patterns as a function of salt type and concentration, as measured by $X_{total\ salt}$.

3.1. Textures

Figure 1 shows SEM images of a starting calcite crystal (Fig. 1A) and several run-products displaying different textures (Figs. 1B-1I). Figures 1B-1F are ordered from lowest solubility to highest solubility. At the lowest solubilities, partly dissolved calcite crystals preserve original shapes but become more rounded. At the highest solubilities, the run-product crystals are highly irregular in shape and display wormy pits and grooves. These textures are observed regardless of the salt added, suggesting that the textures are controlled by solubility rather than solution composition. In low solubility experiments a single large grain was typically recovered (Figs. 1B-1D). In contrast, high solubility experiments typically yielded aggregates of small crystals that were rounded by dissolution (Figs. 1E and 1F). As solubility increased, the

dissolution pits and grooves likely cut channels through the entire width of the crystal, resulting in the aggregates of smaller crystals seen in Figs. 1E and 1F.

The small (~20 μm) euhedral rhombs shown in Fig. 1G are interpreted to be quench material due to their uniform size, high nucleation density, and even distribution on all surfaces (Fig. 1H), including the original calcite crystal (Caciagli and Manning, 2003). Large, skeletal crystals (Fig. 1I) are observed in the highest solubility experiments. These are also interpreted to be quench crystals, consistent with their rapid-growth textures that can be expected to result from the extreme oversaturation upon quenching from very high solubility conditions.

3.2. Precision and accuracy

The 1σ uncertainty in each weighing step was propagated to all solution compositions and solubility values. The resulting 1σ uncertainty in $X_{total\ salt}$ is <1.7 x 10^{-3}. The 1σ uncertainty in m_{CaCO3} when propagated through weighing steps is <1.9 x 10^{-3} molal.

Minimum and maximum calcite solubility measurements are in close agreement when both could be measured, and maximum values are always greater than minimum values (Tables 1 and 2). However, as solubility rises, the difference between maximum and minimum values increases. When contents of the inner Pt capsules were examined, experiments with the highest solubilities qualitatively appeared to contain greater amounts of quench crystals. Therefore, the increasing difference between minimum and maximum solubilities with rising solubility is likely due to larger masses of quench crystals in the inner Pt capsule, which result in lower minimum solubility measurements. Due to difficulties retrieving unbroken calcite crystals, maximum solubility measurements could not always be obtained. In addition to larger discrepancies

between minimum and maximum solubility measurements, high solubility experiments also showed greater scatter.

Where minimum and maximum solubilities could be determined, the range between the two values was larger than the 1σ weighing error in an individual solubility measurement. However, minimum and maximum solubility could not be measured in all cases. I therefore used the average range between minimum and maximum of 0.028 molal ($n = 18$) as a conservative estimate of uncertainty when plotting experiments for which only minimum solubility was determined.

In their study of calcite solubility in H_2O, Caciagli and Manning (2003) encountered problems with new calcite crystals that grew during experiments. These "vapor transport crystals" were not observed in our experiments. This is likely due to the higher solubilities in the current study (Newton and Manning, 2002).

3.3. Equilibrium

To determine the time needed for experiments to reach equilibrium, runs were repeated under identical conditions, but with varying run times. Multiple runs conducted at $X_{LiCl} = 0.023$ showed no systematic variation of calcite solubility with time ≥ 4 hr (Fig. 2). All LiCl experiments were run for a minimum of 4 hr (Tables 1 and 2). Caciagli and Manning (2003) showed that in pure H_2O equilibrium was reached at 12 hours, therefore all other experiments were run for a minimum of 12 hours.

3.4. Solubility in H₂O

A single experiment was conducted in pure water (Table 1) for the purposes of comparison to the results of Caciagli and Manning (2003). I obtained a solubility measurement of 0.016 ± 0.028 molal, which agrees well with their value of $0.021 \pm .005$ molal.

3.5. Solubility in single-salt solutions

The first set of experiments was conducted using aqueous solutions containing a single salt (Table 1). Total salt mole fraction was varied from low concentration to saturation with the respective halide mineral. Figure 3 shows variation of calcite solubility with total salt mole fraction for aqueous solutions containing KCl, NaCl, and LiCl. In all cases, calcite solubility displayed quadratic growth with increased total salt mole fraction (Fig. 3).

Experiments at high LiCl concentration yielded very high calcite solubility, and display significantly more scatter as discussed above. Due to the increased scatter, the three highest concentration LiCl experiments were not considered in regressions. These experiments are shown as unfilled triangles in Fig. 3.

In NaCl and KCl solutions, calcite solubility increased until, at high $X_{total\ salt}$, no further change in calcite solubility was observed (Fig. 3). This is interpreted to reflect salt saturation. Where nominal $X_{total\ salt}$ in the starting fluid is greater than the saturating concentration, no further solubility increase can occur because the solution composition must remain constant and all additional salt simply increases the volume of halite (NaCl) or sylvite (KCl) grown during the experiment (e.g., Aranovich and Newton, 1996). Figure 3 shows that LiCl saturation was not attained.

A single experiment was conducted in a CsCl solution in order to observe the relation between cation size and calcite solubility. Calcite solubility in CsCl at $X_{CsCl} = 0.09$ is 0.079 molal, lower than that in LiCl, NaCl, or KCl at the same $X_{total\ salt}$ (Table 1).

3.6. Solubility in mixed-salt solutions

A second set of experiments examined how mixing salts affects calcite solubility (Table 2). Mixtures included 1:1 molar ratios of two salts: NaCl-KCl, NaCl-LiCl, and KCl-LiCl. Figure 4 shows variation of calcite solubility with total salt mole fraction. Similar to single-salt aqueous solutions, calcite solubility in two-salt aqueous solutions increased exponentially with increasing salt mole fraction (Fig. 4). At any given total salt mole fraction, calcite solubility in the mixed-salt solution lies at a value between that in the end member single-salt solutions of which the solution is comprised (Fig. 4).

In the NaCl-KCl solution (Fig. 4A), calcite solubility continued to increase to $X_{total\ salt} >$ 0.8. Saturation in the NaCl-KCl solution differed from the single-salt solutions, where a constant solubility is attained at $X_{total\ salt}$ equal to or greater than that of salt saturation. Scott (1932) investigated the effects of adding a second salt to solution had on saturation of both salts. He showed that in the NaCl-KCl-H_2O system, both salts will saturate at lower concentrations in a mixed solution compared to a solution comprising only a single salt. Figure 3 shows that in single-salt solutions, NaCl and KCl saturate at about $X_{total\ salt} = 0.35$ and $X_{total\ salt} = 0.45$ respectively. Therefore in a 1:1 molar ratios of NaCl-KCl we would expect to see NaCl saturate at $X_{total\ salt} < 0.7$ and KCl to saturate at $X_{total\ salt} < 0.9$. Figure 4A shows that at around $X_{total\ salt} =$ 0.6 the curve changes concavity, this is likely where NaCl has become saturated. As more NaCl and KCl is added in a 1:1 molar ratio, KCl concentration increases while NaCl is fixed at its

saturation concentration. This likely results in the saturation curve seen in Fig. 4A. LiCl-NaCl and LiCl-KCl mixtures behave similarly to NaCl-KCl, although saturation was not reached in either case (Figs. 4A and 4B).

Another set of experiments was conducted in two-salt solutions by holding $X_{total\ salt}$ constant but varying the proportion of the two salts (Table 2; Fig. 5). The first experiments of this set were conducted at $X_{total\ salt} = 0.18$ to determine calcite solubility variability when relative salt proportions were changed while total salt mole fraction was held constant. Figure 5A shows variation of calcite solubility with NaCl / (NaCl + KCl). As NaCl / (NaCl + KCl) varies from 0 to 1 calcite solubility changes from calcite solubility in a pure KCl solution to that in a pure NaCl solution. Figure 5 shows that calcite solubility does not vary linearly with NaCl / (NaCl + KCl).

Experiments were also conducted with solutions comprising three salts (KCl, NaCl, LiCl) (Table 2). Figure 5A shows experiments in which the mole fraction of LiCl relative to total salts (η_{LiCl}) is kept constant at 0.33, while varying NaCl / (NaCl + KCl) at $X_{total\ salt} = 0.18$. Similar experiments were also conducted along LiCl-NaCl and LiCl-KCl joins (Figs. 5B and 5C). Mixing experiments in three-salt solutions behaved in a similar fashion to those in two-salt solutions.

4. DISCUSSION

4.1. Dependence of calcite solubility on $X_{total\ salt}$

The rise in calcite solubility with total salt mole fraction (Fig. 3) suggests a quadratic dependence of calcite solubility on total salt mole fraction (Newton and Manning, 2002). Figure

6 shows that calcite solubility is linearly dependent on the square of total salt mole fraction.

Least-squares regressions of the salt-undersaturated solubility results give:

$$m_{CaCO_3,KCl} = 1.715X_{KCl}^2 + 0.079 \tag{7}$$

$$m_{CaCO_3,NaCl} = 4.581X_{NaCl}^2 + 0.079 \tag{8}$$

$$m_{CaCO_3,LiCl} = 27.043X_{LiCl}^2 + 0.079 \tag{9}$$

The correlation coefficients for Eqs. (7)-(9) are 0.985, 0.999, and 0.995, respectively. Equations
(7)-(9) reproduce the experimental results with standard errors of estimates of 0.015 molal, 0.006
molal, and 0.029 molal respectively. The intercepts at $X_{total\ salt} = 0$ were fixed at 0.079, which
corresponds to the average intercept derived from regressing each set of results separately, with a
standard deviation of 0.008. Intercepts were fixed so that regressions could be used in mixing
models discussed below. The high correlation coefficients show that fixing the intercepts at
0.079 has negligible effects on fitting of curves.

Regressions analogous to Eqs. (7)-(9) were derived for the 1:1 molar ratio of two-salt
mixtures:

$$m_{CaCO_3,NaCl:KCl} = 2.642X_{total\ salt}^2 + 0.079 \tag{10}$$

$$m_{CaCO_3,LiCl:KCl} = 12.452X_{total\ salt}^2 + 0.079 \tag{11}$$

$$m_{CaCO_3,LiCl:NaCl} = 14.650X_{total\ salt}^2 + 0.079 \tag{12}$$

The correlation coefficients for Eqs. (10)-(11) are 0.988, 0.986, and 0.997, respectively.
Equations (10)-(11) reproduce the experimental results with standard errors of estimates of

0.036 molal, 0.012 molal, and 0.012 molal respectively. Intercepts were forced to 0.079 as in Eqs. (7)-(9).

4.2. Solubility at $X_{total\ salt} < 0.05$

Figure 7 shows calcite solubility at very low $X_{total\ salt}$. Three experiments were conducted at $X_{total\ salt} < 0.05$: one in pure H_2O, one at $X_{total\ salt} = 0.028$ in H_2O-KCl, and one at $X_{total\ salt} = 0.036$ in H_2O-NaCl-KCl. All yielded solubility lower than that predicted by the fitted trends, and instead appear to lie on a separate trend. This suggests that there are likely two different regions where the dominant species differ, resulting in different variation of calcite solubility with salt concentration. $X_{total\ salt} = 0.05$ is used as an estimate for where this change in behavior occurs, although it may occur at a slightly lower or higher $X_{total\ salt}$. Fein and Walther (1989) studied calcite solubility and speciation in NaCl-H_2O solutions and inferred that solutes were fully dissociated at low salt concentrations, but at least partly associated (e.g., $CaCl^+$) at higher salt concentrations. Changes in the dominant species may account for the observed change in trend of calcite solubility at low salt concentrations. More detailed study of the solubility patterns at low $X_{total\ salt}$ are required to more quantitatively evaluate the inferred transition. All following discussion applies only to solubilities at $X_{total\ salt} > 0.05$.

4.3. Solubility at $X_{total\ salt} > 0.05$

Figure 3 shows that increasing the concentration of KCl, NaCl, or LiCl greatly enhances calcite solubility. The most concentrated LiCl solution dissolved nearly 3 moles of $CaCO_3$ per kg of H_2O, which corresponds to ~13 wt%. Calcite solubility in pure H_2O at 700 °C and 8 kbar is about 0.02 molal. Thus, in the most concentrated LiCl solution measured, calcite solubility is

enhanced by nearly 150 times relative to pure H_2O. At NaCl and KCl saturation, calcite

solubilities are about 0.8 and 0.4 molal respectively, or about 40 and 20 times that in pure H_2O

respectively. These results demonstrate the potential for saline brines to transport and redistribute

significant amounts of C by dissolution of calcite.

4.4. Dissolution Mechanism

Figures 3 shows that calcite solubility increases with increasing salt concentration to salt

saturation. This relationship suggests that there is a solution reaction between dissolved $CaCO_3$

and dissolved salts, which enhances the calcite solubility (Newton and Manning, 2002). The fact

that salting-in behavior persists until salt saturation suggests that H_2O is not involved in the

reaction. If it were, the decreasing H_2O activity with increasing salt mole fraction would inhibit

calcite solubility in concentrated solutions (Newton and Manning, 2002), which is not observed.

Therefore heterogeneous and homogeneous reactions that depend on H_2O activity, such as:

$$CaCO_3 + 2H^+ = Ca^{+2} + H_2O + CO_2 \tag{13}$$

and

$$CO_2 + H_2O = H^+ + HCO_3^- \tag{14}$$

do not dominate calcite dissolution in salt solutions at high $X_{total\ salt}$.

Newton and Manning (2002) concluded that for the range of concentration considered,

solutions containing high total NaCl at 800 °C and 10 kbar, the calcite-solution equilibrium

could be described by:

20

$$CaCO_3 + 2\ NaCl_{aq} = CaCl_{2,aq} + Na_2CO_{3,aq} \tag{15}$$

At high P and T, the activity of NaCl is approximately equal to the square of its mole fraction (Aranovich and Newton, 1996), so if the dissolution reaction of the form of Eq. (15) is applicable, calcite solubility should be proportional to the squared NaCl mole fraction. Equations (7)-(12) indicate that this proportionality holds for calcite solubility in one-salt and two-salt solutions. This is highlighted in Fig. 6 where results from one-salt solutions are plotted as a function of the square of total salt mole fraction. Behavior of calcite solubility in KCl and LiCl solutions is similar to that in NaCl solutions, which suggests that the following equilibria also apply:

$$CaCO_3 + 2\ KCl_{aq} = CaCl_{2,aq} + K_2CO_{3,aq} \tag{16}$$

$$CaCO_3 + 2\ LiCl_{aq} = CaCl_{2,aq} + Li_2CO_{3,aq} \tag{17}$$

$$CaCO_3 + 2\ CsCl_{aq} = CaCl_{2,aq} + Cs_2CO_{3,aq} \tag{18}$$

Figure 8 shows that at any given salt mole fraction, calcite solubility increased with decreasing cation radius of the participating salt (Shannon, 1976) i.e. $Li^+ > Na^+ > K^+ > Cs^+$. Aranovich and Newton (1997) investigated the activity of KCl in H_2O solutions at high pressures and temperatures and found them to be lower than NaCl activities when pressure, temperature and salt mole fraction were equal. Decreasing salt activity with decreasing cation radius may explain the trend seen in Fig. 8.

4.5. Calcite solubility variability with cation hardness

Another possible explanation for the observed increase in calcite solubility with decreasing cation size (Fig. 8) is the stability of the aqueous complexes formed in Eqs. (15)-(18). In Eqs. (15)-(18) the salt cation (Cs^+, K^+, Na^+, Li^+) forms an aqueous complex with the carbonate anion. Therefore, the stability of the aqueous complexes in order from least to greatest would be $Cs_2CO_{3,aq} < K_2CO_{3,aq} < Na_2CO_{3,aq} < Li_2CO_{3,aq}$. This trend in stability can be predicted using Pearson's hard-soft acid-base principles, which state that hard acids form stronger bonds with hard bases and soft acids form stronger bonds with soft bases. The carbonate ion is a hard base, so it should form stronger bonds with harder acids. Parr and Pearson (1983) defined chemical hardness as:

$$h = \tfrac{1}{2}(I\text{-}A) \tag{19}$$

where h is hardness, I is ionization energy, and A is electron affinity. According to Eq. (19), cations considered in this study increase in hardness as $Cs^+ < K^+ < Na^+ < Li^+$. As illustrated in Fig. 9, calcite solubility increases with the hardness of the salt cation. Thus, the increased calcite solubility in solutions containing smaller cations is likely due in part to harder cations (smaller cations) forming more stable complexes with the hard carbonate ion. This suggests that calcite solubility in aqueous alkali chloride solutions may be predictable using the relationship between calcite solubility and chemical hardness of the alkali.

4.6 Predicting calcite solubility in multi-salt solutions

      The experimental data can be used to derive general relations for calcite solubility in two-salt and three-salt solutions. Below I develop a simple empirical scheme for the solubility of calcite at 700 °C, 8 kbar, $X_{total\ salt} > 0.05$, and a range of salt ratios.

4.6.1. Two-salt solutions

      The approach for empirical prediction of calcite solubility in two-salt solutions at all molar salt ratios can be developed using a 1:1 molar mixture of NaCl-KCl as an example. Figure 10 shows that for 1:1 molar ratio mixtures of NaCl and KCl, calcite solubility varies linearly with the square of total salt mole fraction, as in single-salt solutions. If the salt mixing was similar to a simple mechanical mixture, then calcite solubility could be calculated N_i of the respective end members. That is, if solubility in end members A and B is:

$$m_A = y_A(X_A)^2 + y_0 \tag{20}$$

$$m_B = y_B(X_B)^2 + y_0 \tag{21}$$

where $m_i = m_{CaCO3}$ in a single-salt solution i-H$_2$O, y_i is the fitted solubility dependence on X_i (slope) in i-H$_2$O solutions [Eqs. (7)-(12); Fig. 10], and y_0 is the solubility in pure H$_2$O, then solubility in an A-B salt solution would be:

$$m_{A:B} = N_A m_A + N_B m_B \tag{22}$$

If $A{:}B$ is 1:1, then $N_A = N_B = 0.5$ in Eq. (22). However, Fig. 10 shows that although the molar NaCl:KCl ratio is 1:1, calcite solubility at a given $X_{total\ salt}$ is not one half the difference between that in the respective single-salt solutions (H$_2$O-NaCl and H$_2$O-KCl), so Eq. (22) can not be used. Instead, a correction factor $\bar{x}_i$ can be defined for any two-salt mixture such that

$$m_{A:B} = \bar{x}_{A(A:B)}m_A + \bar{x}_{B(A:B)}m_B \tag{23}$$

In an A-B solution, $\bar{x}_{A(A:B)}$ varies from 0 at $N_A = 0$ ($N_B = 1$) to 1 at $N_A = 1$ ($N_B = 0$), and

$$\bar{x}_{B(A:B)} = 1 - \bar{x}_{A(A:B)} \tag{24}$$

Experiments yield a regressed value of calcite solubility $m^*_{A:B}$ at a particular ratio $A{:}B$ (here 1:1), which can be used to calculate $\bar{x}_{A(AB)}$ for that composition (indicated with a *):

$$\bar{x}^*_{A(AB)} \equiv \frac{m^*_{A:B} - m_B}{m_A - m_B} \tag{25}$$

In the 1:1 NaCl-KCl solutions studied here, $\overline{x}_{NaCl(NaCl:KCl)} = 0.324$ and $\overline{x}_{KCl(NaCl:KCl)} = 0.676$. Since the fits are linear with the square of salt mole fraction (Fig. 10), $\overline{x}_{NaCl(NaCl:KCl)}$ and $\overline{x}_{KCl(NaCl:KCl)}$ are constant for a 1:1 molar mixture of NaCl and KCl at all $X_{total\ salt}$. Combining the constraints from end-member solutions with the assumption that $\overline{x}_{A(A:B)}$ is described by a simple second order polynomial of the form:

$$\overline{x}_{A(AB)} = a_1 N_A + a_2 N_B^2 \tag{26}$$

yields a function describing the variation of $\overline{x}_{NaCl(NaCl:KCl)}$ with N_{NaCl} in all NaCl-KCl solutions (Fig. 11). For NaCl-KCl solutions, this equation is:

$$\overline{x}_{NaCl(NaCl:KCl)} = 0.295 N_{NaCl} + 0.705 N_{NaCl}^2 \tag{27}$$

At any N_{NaCl} in NaCl-KCl solutions, $\overline{x}_{KCl(NaCl:KCl)}$ can be derived from Eq. (24).

Using this approach, functions describing $\overline{x}_{A(AB)}$ in the other two-salt solutions were derived:

$$\overline{x}_{LiCl(LiCl:NaCl)} = 0.793 N_{LiCl} + 0.207 N_{LiCl}^2 \tag{28}$$

$$\overline{x}_{LiCl(LiCl:KCl)} = 0.695 N_{LiCl} + 0.305 N_{LiCl}^2 \tag{29}$$

For each two-salt system, values of $\overline{x}_{B(A:B)}$ can again be calculated using Eq. (24).

Using the $\overline{x}_i$ values derived above, calcite solubilities can be predicted in all two-salt solutions at the experimentally studied salt concentrations. Figure 5 shows that the calculated solubilities reproduce the experimental data with high fidelity at all molar salt ratios and all X$_{total}$ $_{salt}$. This is illustrated in Fig. 12, which shows measured calcite solubility in two-salt solutions versus calcite solubility predicted from Eq. (23) and the values of $\overline{x}_i$ derived above. The data in Fig. 12 cluster around the 1:1 line, with an average deviation of 6.14%.

4.6.2. Three-salt solutions

The success of the predictive scheme developed for two-salt solutions suggests that the same approach can be generalized to three-salt solutions. If correct, we can write:

$$m_{CaCO_3} = \sum_i \bar{x}_i m_i \tag{30}$$

where m_i is again calcite solubility in a solution containing only salt i. A simple approach to deriving values of $\bar{x}_{A(ABC)}$ is to use $\bar{x}_{A(AB)}$ in a C-free solution and then correct for the effect of addition of salt C. That is:

$$\bar{x}_{A(ABC)} = \bar{x}_{A(AB)} \tag{31}$$

$$\bar{x}_{C(ABC)} = N_{A(AB)}\bar{x}_{C(AC)} + N_{B(AB)}\bar{x}_{C(BC)} \tag{32}$$

$$\bar{x}_{B(ABC)} = 1 - \bar{x}_{A(ABC)} - \bar{x}_{C(ABC)} \tag{33}$$

where η_i must be substituted for N_i, when calculating $\bar{x}_{A(AB)}, \bar{x}_{C(AC)},$ and $\bar{x}_{C(BC)}$.

Calcite solubility was calculated in three-salt solutions using Eqs. (7)-(9) and (30)-(33), with A = NaCl, B = KCl, and C = LiCl. Figure 13 shows measured vs. calculated calcite solubility in three-salt solutions. The close fit to the 1:1 line shows that this method of predicting calcite solubility is accurate, with an average deviation of 1.32%. Five experiments were conducted at $X_{total\ salt}$ = 0.18 (Table 1). Fig. 14 shows these experiments on a ternary diagram with contours of constant CaCO$_3$ molality.

The success of the predictive scheme developed above implies that calcite solubility in solutions comprising H$_2$O-NaCl-KCl-LiCl can be predicted over a wide range of total salt mole

fractions. Figures 15A-15F show ternary diagrams with contours of constant calcite solubility at different total salt mole fractions. All figures have the same contour interval and color scale to illustrate how calcite solubility changes with changes in total salt mole fraction. Figure 15 shows that calcite solubility greatly increases with increasing salt mole fraction, and also that the range of calcite solubility greatly increases with increasing salt mole fraction. In addition, it is likely that the simple mixing equations can be extended to n-salt solutions.

4.7. Geologic Applications

Studies on fluid inclusions reveal that salinity of geologic fluids can range from dilute to near saturation (Fu et al., 2001; Yardley and Graham 2002; Manning and Aranovich, in press). Newton and Manning (2002) showed that addition of NaCl to H_2O exponentially increases calcite solubility. However, metamorphic fluids are typically contain additional salts (e.g., Yardley and Graham 2002). The present results show that, regardless of the chloride salt mixture, saline brines have the capacity to dissolve significantly more $CaCO_3$ than pure H_2O, and that the exponential dependence of calcite solubility on salt content is a feature of all studied H_2O-salt systems.

Thus, this study also suggests that when considering calcite solubility in saline fluids, all salt species should be considered. Many times salinity is treated as NaCl wt % equivalent, treating all salt species as NaCl (Yardley and Graham 2002). The present study shows that calcite solubility will differ depending on the cations present in solution. Fluid inclusions in eclogites from the Monviso meta-ophiolitic complex in the French-Italian Western Alps contain daughter crystals of both halite and sylvite (Philippot and Selverstone, 1991). In fluids such as this which contain high concentrations of both NaCl and KCl, it may be important to consider

27

both when predicting calcite solubility. For example, if a fluid at 700 °C and 8 kbar consisted of a 1:1 molar mixture of NaCl and KCl, the model presented would predict a calcite solubility of 0.185 molal. However, if all salts were treated as NaCl, the predicted calcite solubility would be 0.262 molal, which overestimates calcite solubility by 30%. Therefore, to provide better constraints on calcite solubility, all salt species present in solution should be considered. Shmulovich et al. (2006) found that different salt species have different effects on quartz solubility. When considered together with results of the present work, it is clear that knowledge of the relative abundance of dissolved salts is important for prediction of mineral solubility in metamorphic fluids.

4.8 Conclusions

The results of this study present several conclusions.

(1) Calcite solubility follows a consistent, predictable behavior with increasing salt concentration in aqueous KCl, NaCl, and LiCl solutions.

(2) Calcite solubility in mixed salt solutions is not accurately predicted by assuming ideal mixing of salts in solution, however the present study provides a method to make corrections for mixing and accurately predict calcite solubility in mixed-salt solutions.

(3) Calcite solubility in saline solutions is enhanced relative to pure H_2O by complexation of the Ca^{2+} and CO_3^{2-} ions with the dissolved salt ions. The observed trend of calcite solubility increasing with decreasing cation size, i.e. CsCl < KCl < NaCl < LiCl, is likely due to the CO_3^{2-} ion forming more stable complexes with harder ions as predicted by Pearson's hard-soft acid-base principles.

These findings allow for prediction of calcite solubility over a wide range of fluid compositions relevant to natural systems.

4.9 Future Study

Calcite dissolution in dilute salt solutions ($X_{total\ salt}$ <0.05) deviates from the trends extrapolated from $X_{total\ salt}$ > 0.05 (Fig. 7). These low salt concentration fluids are important in natural systems, therefore more studies should be conducted on low concentration fluids. The present study illustrates how calcite solubility is affected by composition at 700 °C and 8 kbar. In order for these results to be more generally applicable, pressure and temperature effects should be studied for KCl and LiCl following Caciagli and Manning (2003) and Newton and Manning (2002). With constraints on calcite solubility over a wide range of compositions as well as a wide range of pressures and temperatures, constraints on carbon transport in geologic fluids will become much better. Also, geologic fluids are not comprised solely of alkali halides; $CaCl_2$, and $MgCl_2$ are very important salts, and the effects of salts such as these should also be studied. The results of the present study suggest that mixing of salts in aqueous fluids is non-ideal, and while the present study provides an empirical method to correct for non-ideality and accurately predict calcite solubility in mixed salt solutions, it does not provide a physical explanation of non-ideality upon mixing. Therefore non-ideal mixing of salts in solution may deserve more attention.

Table 1. Calcite solubility measurements at 700 °C, and 8 kbar, in H_2O and single-salt solutions

Expt. Number	Time (hours)	Salt in (mg)	H_2O in (mg)	H_2O out (mg)	$X_{total\ salt}$ in	Capsule in (mg)	Capsule out (mg)	Calcite in (mg)	Calcite out (mg)	Minimum $CaCO_3$ solubility (molal)	Maximum $CaCO_3$ solubility (molal)
Pure H₂O											
W-1	23	0.000	16.996	17.043	0.000	49.529	49.502	0.479	-	0.016	-
KCl											
K-1	22	2.751	22.723	-	0.028	56.615	56.522	0.468	-	0.041	-
Y-5	27	6.580	29.810	-	0.051(1)	61.706	61.452	3.277	-	0.085(1)	-
Y-1	24	13.874	30.213	-	0.100	64.243	63.961	2.445	2.018	0.093(1)	0.141(1)
Y-2	72	30.573	30.486	-	0.195	60.946	60.474	3.142	2.527	0.155(1)	0.202(1)
MT-4	17	15.557	15.178	-	0.199	52.500	52.271	0.615	-	0.151(1)	-
Y-3	23	53.238	29.985	-	0.300	70.881	70.174	3.578	2.854	0.236	0.241
Y-4	25	41.432	14.596	-	0.407	62.145	61.628	3.945	-	0.354(1)	-
J-4	25	47.575	16.352	-	0.413	55.567	54.971	1.271	-	0.364(1)	-
J-8	22	54.224	16.175	-	0.448	49.054	48.371	1.077	0.380	0.422(1)	0.431(1)
Y-6	22	61.794	15.558	-	0.490	62.313	61.661	2.327	-	0.419(1)	-
NaCl											
J-6	24	11.201	30.453	-	0.102	53.870	53.501	1.003	0.600	0.121(1)	0.132(1)
MT-1	23	16.220	20.029	20.031	0.200	49.171	48.662	1.269	-	0.253(1)	-
J-7	25	32.768	31.394	-	0.243	56.207	55.147	1.906	0.800	0.337	0.352
J-10	22	53.457	30.282	-	0.352	62.475	60.529	2.690	0.673	0.642	0.665
J-12	21	32.428	14.606	-	0.406	57.934	56.826	2.490	-	0.758	-
J-16	24	42.328	14.748	-	0.469	63.505	62.346	2.069	-	0.785	-
J-18	24	40.268	9.343	-	0.571	47.659	46.942	1.551	-	0.767(1)	-
LiCl											
L-27	24	1.144	21.296	21.836	0.022(2)	50.562	50.374	0.646	-	0.088(2)	-
L-9	4	1.444	25.520	26.009	0.023(1)	48.969	48.756	1.186	0.975	0.084(1)	0.083(1)
L-19	8	1.918	33.985	34.511	0.023(1)	52.696	52.426	0.997	0.695	0.079(1)	0.086(1)
L-26	30	1.296	23.679	24.268	0.023(1)	54.670	54.455	0.638	-	0.091(1)	-

L-18	24	1.658	20.896	-	0.033(1)	50.114	49.863	0.773	-	0.120(1)	-
L-7	5	3.371	25.162	25.551	0.054	60.837	60.461	3.666	-	0.149(1)	-
L-15	24	3.718	16.154	-	0.089	48.517	48.009	1.206	-	0.314(1)	-
L-8	5	10.023	24.393	24.819	0.149	63.979	62.589	3.140	1.602	0.569	0.630
L-16	23	3.905	9.070	9.299	0.155	61.366	60.694	1.743	-	0.740(1)	-
L-14	23	9.831	18.545	-	0.184	52.850	50.961	2.107	-	1.018	-
L-17	23	4.487	8.425	-	0.185	53.897	53.018	1.625	-	1.043(1)	-
L-10	23	6.244	11.298	12.020	0.190	59.114	57.950	1.822	-	1.029	-
L-11	5	5.585	8.170	8.435	0.225	62.703	61.628	2.900	-	1.314(1)	-
L-12	17	6.390	7.360	-	0.270	65.337	63.735	2.365	-	2.174(1)	-
L-13	19	9.796	10.263	-	0.289	60.497	57.553	1.763	-	2.865	-
CsCl											
CS-1	23	15.341	16.944	17.551	0.088	53.028	52.897	0.060	-	0.079	-

Explanation: Table of measurements used to calculate calcite solubility for experiments in pure H_2O and solutions comprising a single salt. "in" and "out" refer to measurement made before and after experiment respectively. H_2O in measurements were used in all calculations. The 1σ weighing uncertainty was propagated through each weighing step. Parenthetical numbers reflect 1σ uncertainty in last digit. Any $1\sigma < 0.0005$ was excluded from table.

Table 2. Calcite solubility measurements at 700 °C, and 8 kbar, in mixed-salt solutions

Expt. Number	Time (hours)	KCl in (mg)	NaCl in (mg)	LiCl in (mg)	H$_2$O in (mg)	H$_2$O out (mg)	X$_{KCl}$ in	X$_{NaCl}$ in	X$_{LiCl}$ in	X$_{total\ salt}$ in	Capsule in (mg)	Capsule out (mg)	Calcite in (mg)	Calcite out (mg)	Minimum CaCO$_3$ solubility (molal)	Maximum CaCO$_3$ solubility (molal)
NaCl-KCl																
J-3	25	2.187	1.576	0.000	27.393	-	0.019	0.017	0.000	0.036(1)	50.995	50.848	1.312	-	0.054(2)	-
Y-7	20	6.935	5.798	0.000	29.026	-	0.052	0.055	0.000	0.107	62.555	62.229	1.795	-	0.112(1)	-
Y-8	23	15.840	13.082	0.000	34.988	-	0.089	0.094	0.000	0.183	62.355	61.721	2.712	2.040	0.181(1)	0.192
MT-3	31	13.533	4.160	0.000	20.256	20.340	0.132	0.052	0.000	0.184	47.981	47.646	0.937	-	0.165(1)	-
MT-2	25	4.044	7.959	0.000	15.219	15.322	0.052	0.132	0.000	0.184(1)	48.694	48.378	0.714	-	0.207(1)	-
J-1	24	13.292	10.678	0.000	16.539	-	0.139	0.143	0.000	0.282	61.508	61.018	1.628	-	0.296(1)	-
J-2	24	20.679	16.343	0.000	16.283	-	0.190	0.191	0.000	0.381	59.804	59.122	2.354	1.504	0.418(1)	0.522
J-5	23	28.267	22.331	0.000	16.318	-	0.227	0.229	0.000	0.457	58.197	57.308	2.459	1.543	0.544	0.561
J-9	22	47.463	37.080	0.000	14.280	-	0.308	0.307	0.000	0.616	58.562	56.963	3.038	-	1.119	-
J-11	23	48.678	37.801	0.000	11.224	-	0.340	0.336	0.000	0.676	59.059	57.560	2.901	1.313	1.334	1.414
J-14	24	37.513	29.691	0.000	5.745	-	0.378	0.382	0.000	0.760	72.378	71.479	2.663	-	1.563(1)	-
J-17	24	41.974	32.778	0.000	3.301	-	0.431	0.429	0.000	0.860	66.214	65.668	0.000	-	1.653(2)	-
KCl-LiCl																
KL-4	23	5.858	0.000	3.250	21.096	20.715	0.059	0.000	0.058	0.117(1)	51.085	50.529	1.111	-	0.263(1)	-
KL-1	23	5.402	0.000	3.389	15.403	-	0.072	0.000	0.079	0.151(1)	59.937	59.397	1.458	-	0.350(1)	-
MT-8	23	10.267	0.000	2.048	14.959	-	0.136	0.000	0.048	0.183(1)	51.887	51.418	0.925	-	0.313(1)	-
MT-9	24	4.346	0.000	6.247	16.491	16.730	0.052	0.000	0.131	0.183(1)	52.775	51.596	1.717	-	0.714	-
KL-3	19	12.569	0.000	6.765	26.291	26.583	0.094	0.000	0.089	0.184	60.342	59.043	1.884	0.537	0.494	0.512
NaCl-LiCl																
NL-3	20	0.000	2.917	2.017	25.917	26.477	0.000	0.032	0.031	0.063(1)	59.489	59.108	0.854	-	0.147(1)	-
NL-2	23	0.000	4.702	2.861	20.023	-	0.000	0.064	0.054	0.117(1)	59.219	58.678	0.775	-	0.270(1)	-
NL-1	30	0.000	5.735	4.265	20.650	20.877	0.000	0.073	0.075	0.148(1)	65.955	65.161	1.846	-	0.384	-
MT-5	29	0.000	8.018	2.410	15.465	15.777	0.000	0.130	0.054	0.184(1)	51.737	51.104	0.968	-	0.409(1)	-
MT-6	15	0.000	3.392	5.906	15.689	-	0.000	0.054	0.130	0.185(1)	53.360	52.264	1.570	-	0.698	-
NL-4	22	0.000	5.638	4.409	14.173	14.431	0.000	0.098	0.105	0.203(1)	57.891	56.906	1.735	-	0.694	-
NaCl-LiCl-KCl																
KLN-7	21	3.452	3.273	1.742	20.057	20.481	0.037	0.045	0.033	0.114(1)	58.236	57.856	1.589	-	0.189(1)	-

32

KLN-8	22	6.120	5.165	1.296	20.890	21.209	0.060	0.065	0.022	0.148(1)	53.088	52.644	1.111	-	0.212(1)	-
KLN-9	21	5.150	1.666	3.163	15.626	16.012	0.066	0.027	0.072	0.166(1)	62.990	62.356	2.229	-	0.405(1)	-
KLN-3	19	9.214	3.313	3.643	21.408	21.448	0.085	0.039	0.059	0.183(1)	50.523	49.737	1.279	0.417	0.367	0.403
KLN-5	22	1.978	2.491	5.401	15.744	-	0.025	0.040	0.119	0.184(1)	58.991	57.978	2.046	-	0.643	-
KLN-2	25	2.027	5.646	2.633	14.873	14.720	0.027	0.096	0.061	0.184(1)	61.029	60.408	0.898	0.262	0.417(1)	0.427(1)
KLN-1	8	4.847	3.671	2.628	15.105	15.076	0.063	0.061	0.060	0.185(1)	55.800	55.254	1.275	-	0.361(1)	-
KLN-4	23	11.304	1.455	3.795	21.111	21.544	0.105	0.017	0.062	0.185(1)	51.901	51.154	1.491	0.723	0.354(1)	0.363

Explanation: Same as table 1, but for experiments comprising multiple salts.
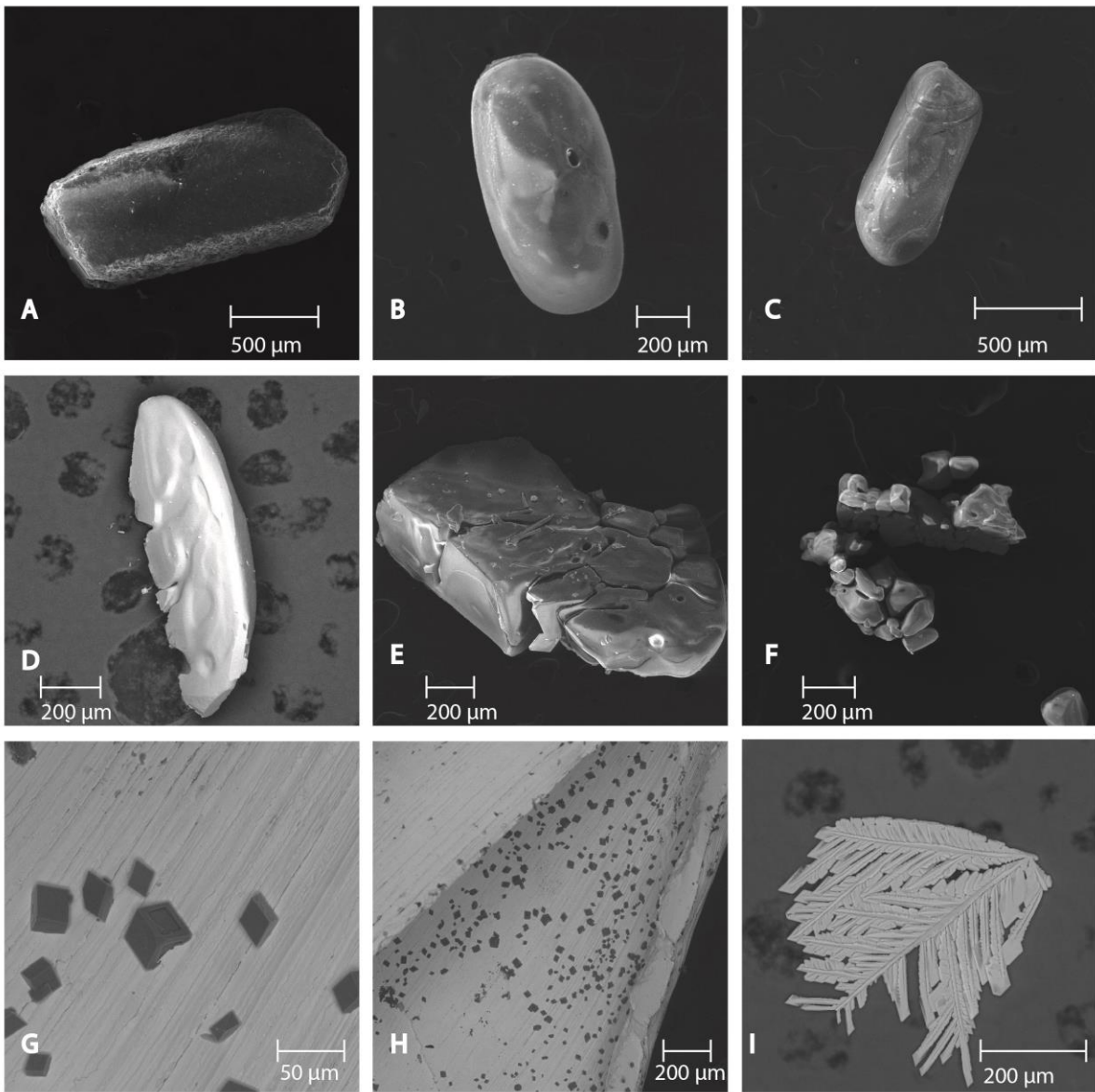
Figure 1. Scanning electron microscope images of starting crystal and run products from selected experiments. B-F are ordered from lowest to highest calcite solubility to illustrate the progression of textures with increasing dissolved $CaCO_3$. (A) Starting crystal (secondary electrons). (B). Dissolution-rounded calcite crystal (run L-19; $m_{CaCO3} = 0.078$; secondary electrons). (C) Dissolution-rounded calcite crystal (run MT-4; $m_{CaCO3} = 0.151$; secondary electrons). (D) Dissolution-rounded calcite crystal showing incipient pits and grooves (run NL-1;

m_{CaCO3} = 0.384; backscattered electrons). (E) Dissolution-rounded calcite crystals displaying numerous, deep pits and grooves (run L-10; m_{CaCO3} = 1.029; secondary electrons). (F) Aggregate of dissolution-rounded calcite crystals. Pits and grooves have cut through the entire crystal and broken it into pieces (run L-11; m_{CaCO3} = 1.314; secondary electrons). (G) Small, euhedral calcite quench crystal on the inner surface of the inner Pt capsule (run NL-3; m_{CaCO3} = 0.147; backscattered electrons). (H) Same as .Fig 1G but lower magnification, showing distribution of calcite quench crystals (backscattered electrons). (I) Skeletal calcite quench crystals observed only in runs with very high solubility, interpreted to be due to strong oversaturation upon quenching (run L-14; m_{CaCO3} = 1.018; backscattered electrons)
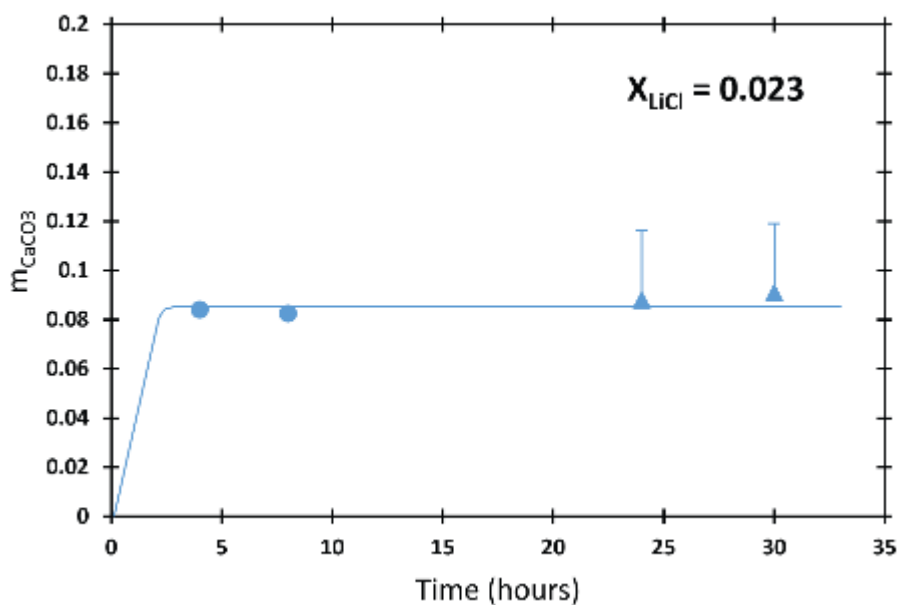
Figure 2. Calcite solubility (molality) vs. experimental duration in H_2O-LiCl solutions at 700 °C, 8 kbar, and $X_{LiCl} = 0.023$. Solubility in molality (m). The absence of systematic variation of calcite solubility with time shows that equilibrium is reached within four hours. Circles represent midpoints between minimum and maximum measured solubility (see text). Triangles represent experiments for which only minimum solubilities were recorded. Error bars are shown where larger than the symbol size; those for average solubilities reflect the range between minimum and maximum values , whereas those for minimum solubilities reflect the average range (0.028 molal) between minimum and maximum values for all experiments in which a maximum value could be measured (see text). Only positive error bars are included on triangles as the triangles themselves represent the minimum value.
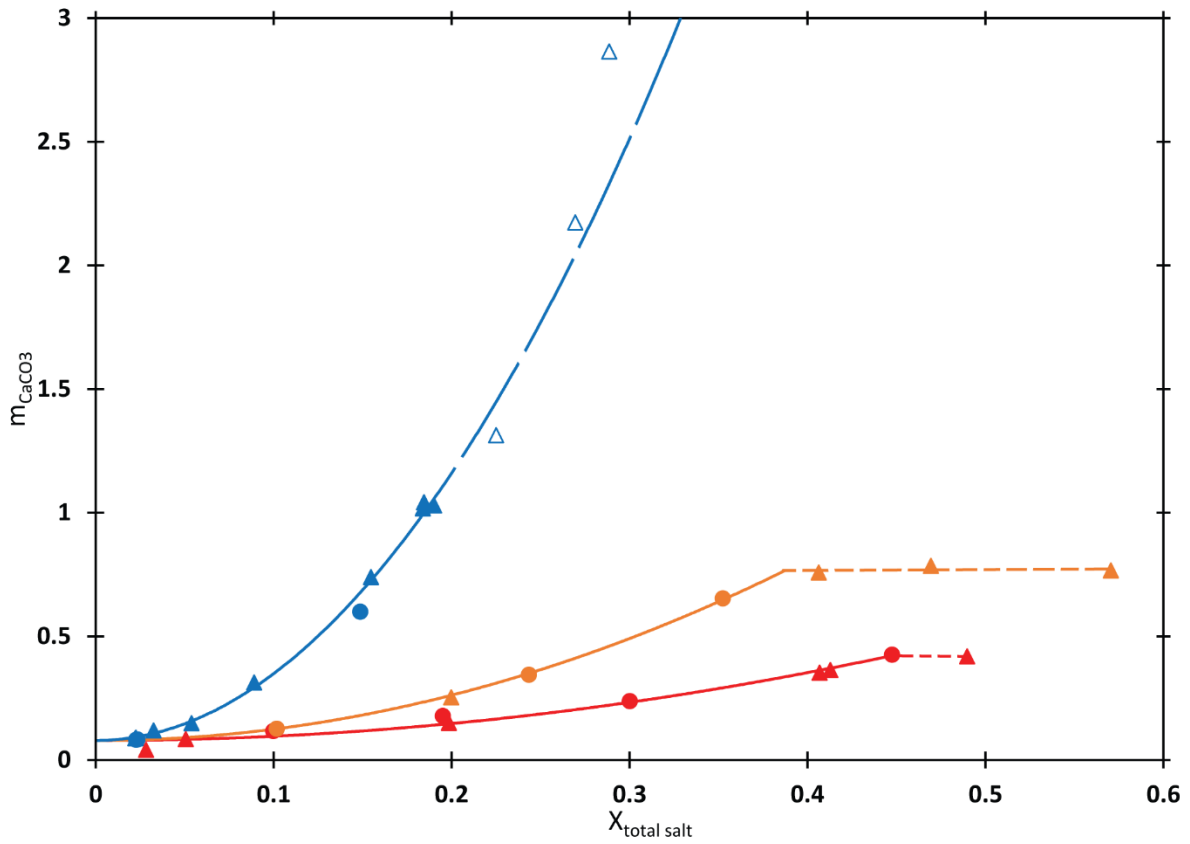
Figure 3. Experimentally determined CaCO$_3$ solubility (molality) vs. total salt mole fraction in single-salt experiments. Symbols as in Fig. 2. Experiments represented with unfilled triangles were not considered in data regression due to significant scatter (see text). Solid lines are based on regressions given in text [Eqs. (7)-(9)]. Short-dashed lines show where salt is saturated. Long-dashed lines show where fit is extrapolated.
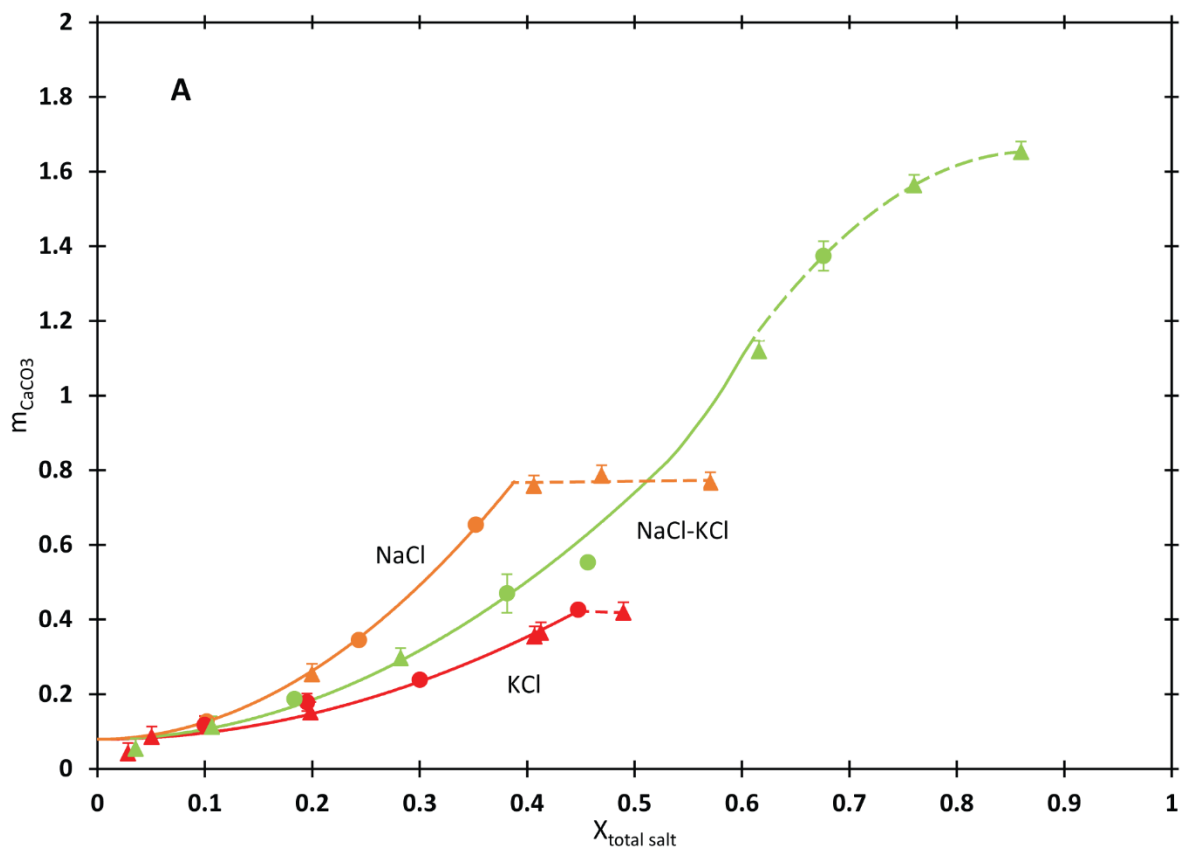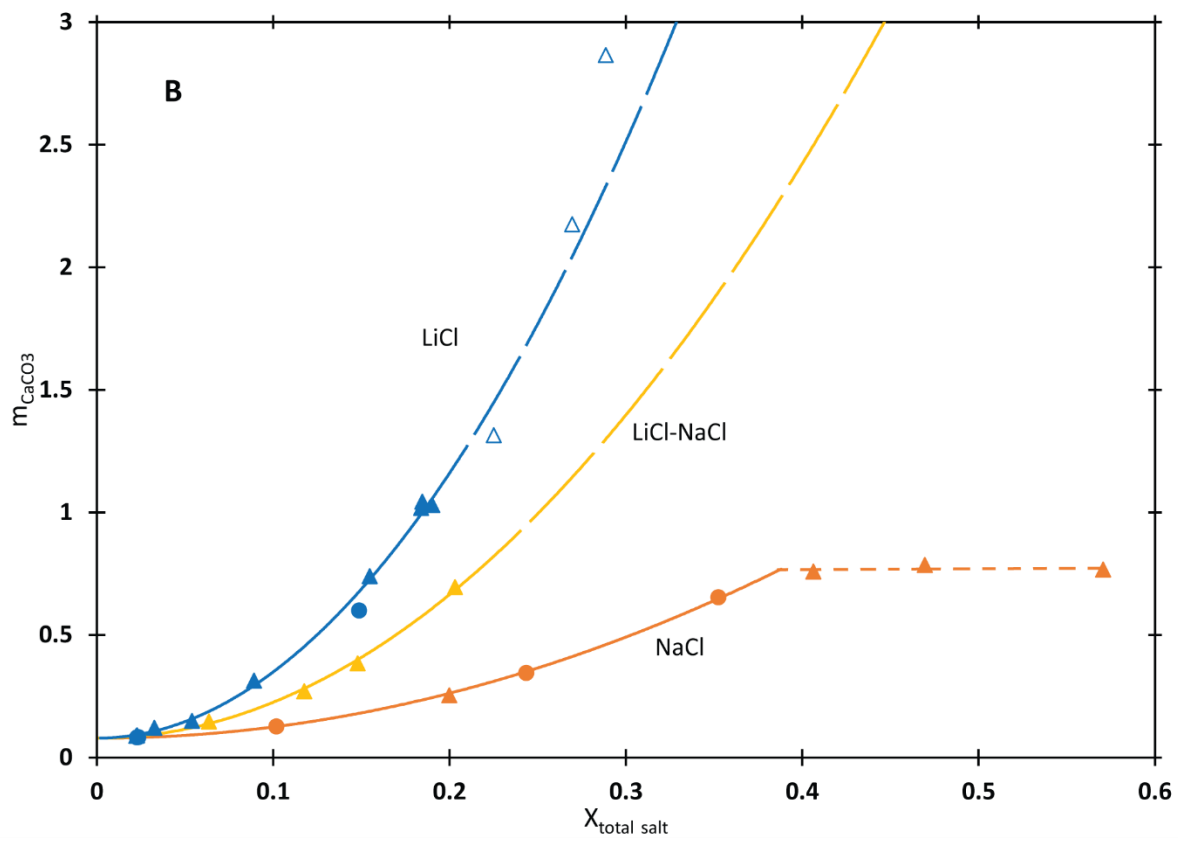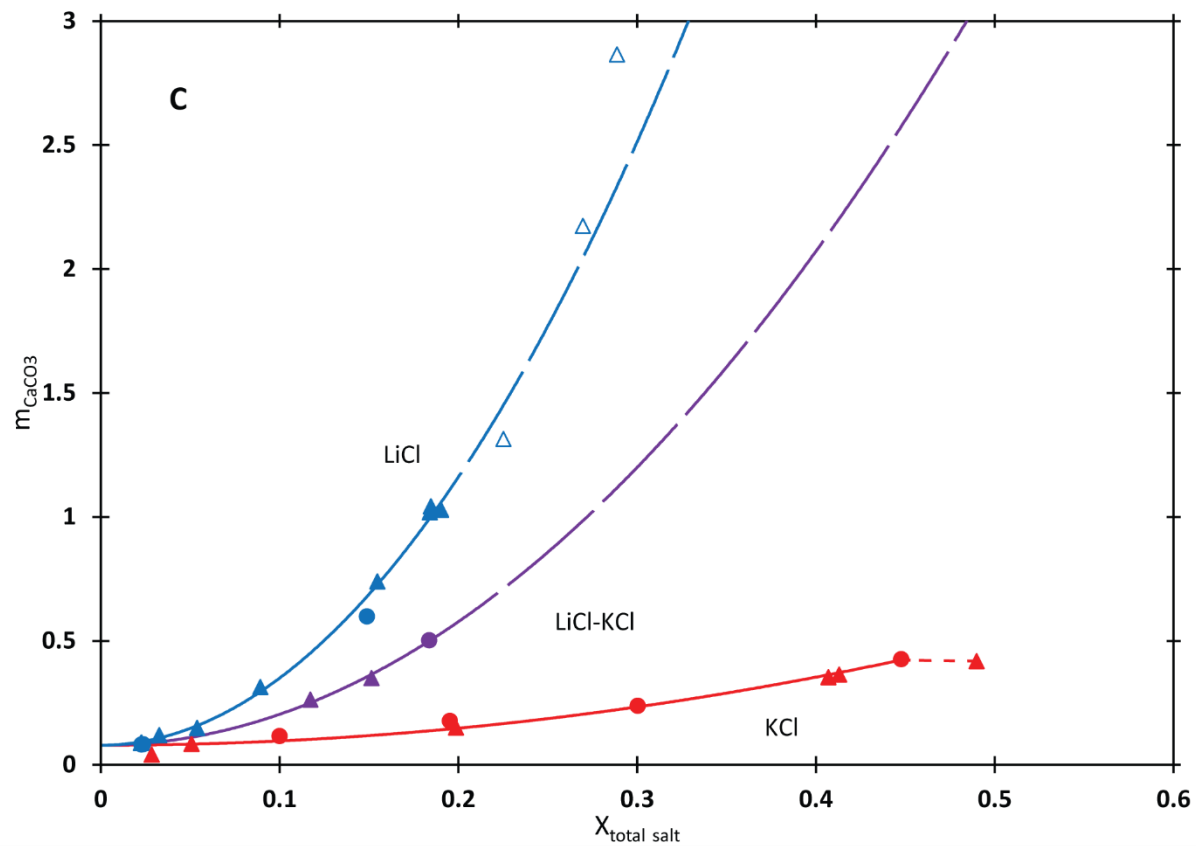
Figure 4. Calcite solubility (molality) vs. total salt mole fraction in two-salt mixtures. (A) 1:1 molar ratio of NaCl and KCl (results in NaCl and KCl, single-salt solutions (Fig. 3) for reference). Note that calcite solubility in the mixture lies between the calcite solubility in the single-salt solutions. (B) 1:1 molar ratio of LiCl and NaCl (results in LiCl and NaCl, single-salt solutions (Fig. 3) for reference). (C) 1:1 molar ratio of LiCl and KCl (results in LiCl and KCl, single-salt solutions (Fig. 3) for reference). Symbols and error bars as in Figs. 2 and 3.

A

$X_{total\ salt}$ = 0.18

η_{LiCl} = 0.33

η_{LiCl} = 0.00

NaCl / (NaCl+KCl)

m_{CaCO3}

B

$X_{\text{total salt}} = 0.18$

$\eta_{KCl} = 0.00$

$\eta_{KCl} = 0.14$

m_{CaCO3}
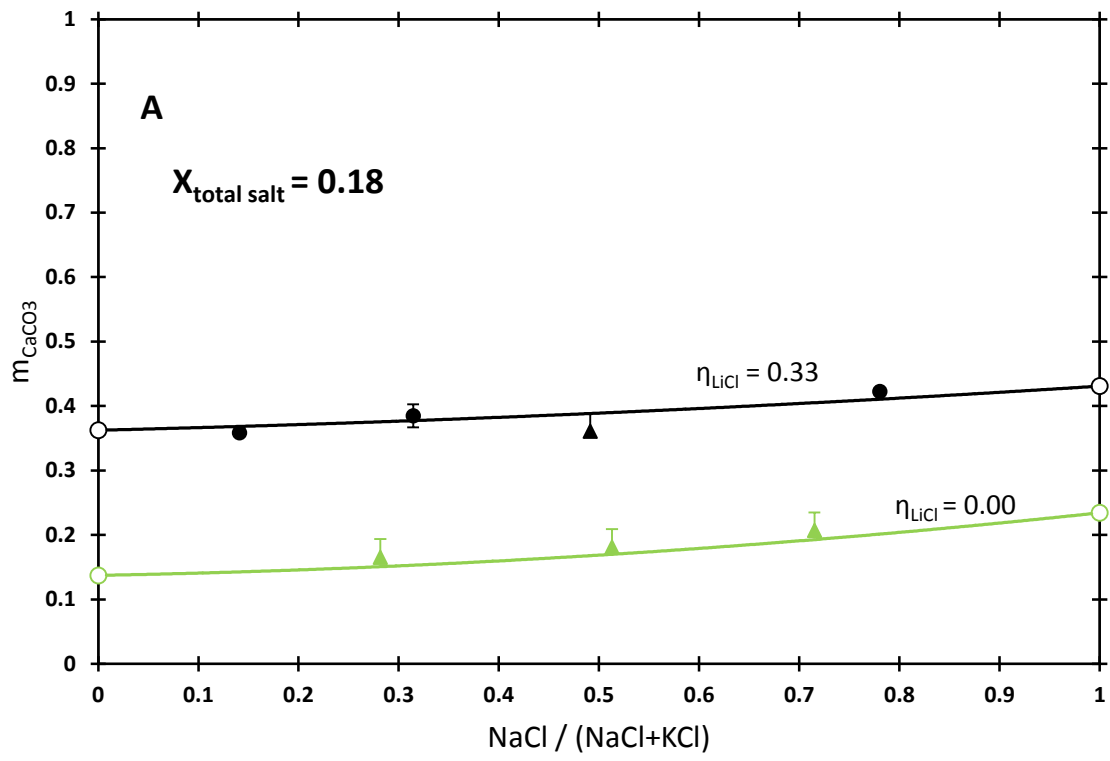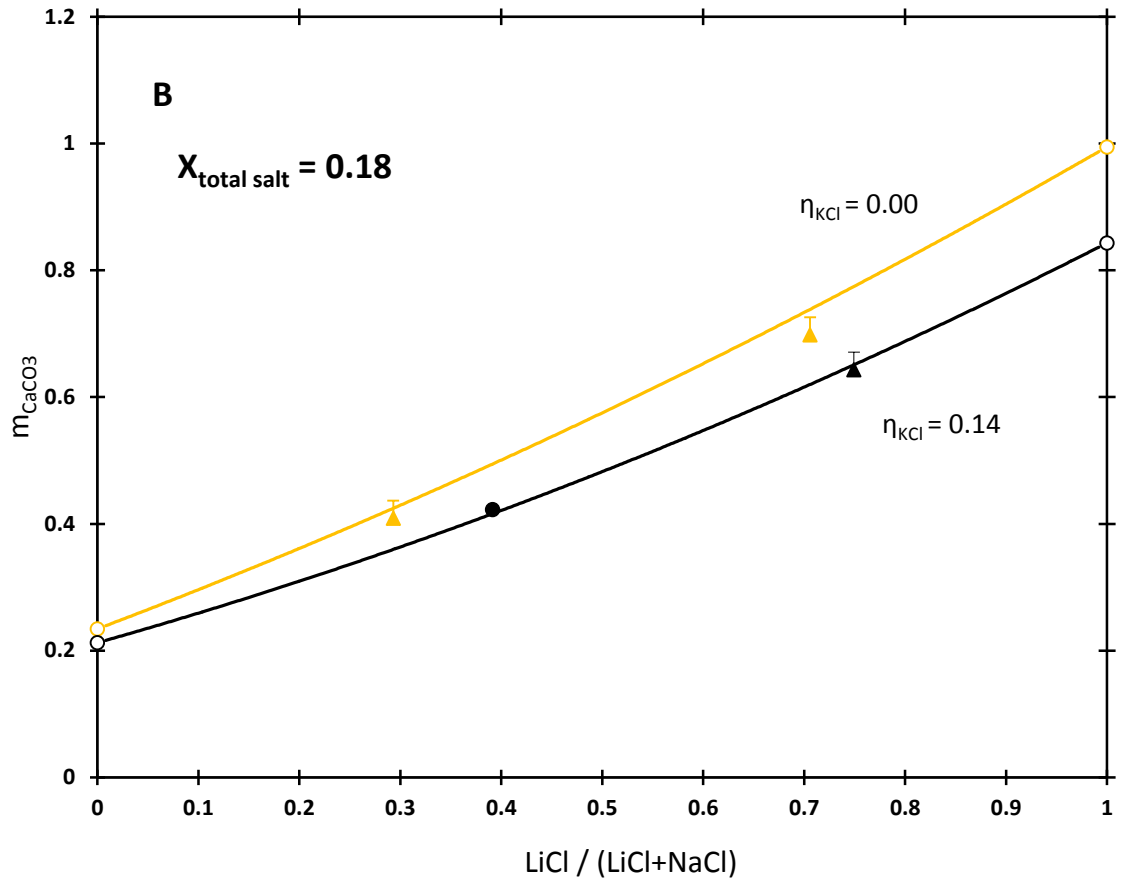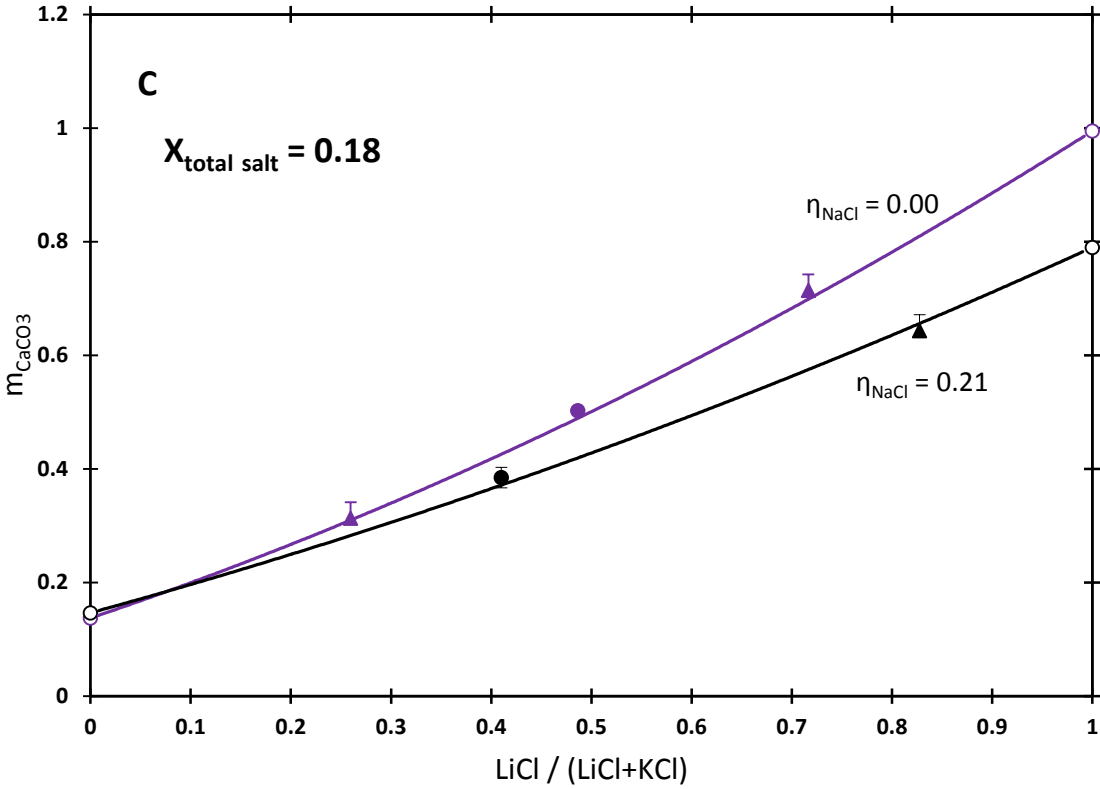
LiCl / (LiCl+NaCl)

Figure 5. Calcite solubility (molality) in three-salt mixtures at $X_{total\ salt} = 0.18$. (A) Solubility variations with molar NaCl / (NaCl + KCL), at $\eta_{LiCl} = 0.00$ (green) and $\eta_{LiCl} = 0.33$ (black). . (B) Solubility variations with molar LiCl / (LiCl + NaCL), at $\eta_{KCl} = 0.00$ (yellow) and $\eta_{KCl} = 0.14$ (black). (C) Solubility variations with molar LiCl / (LiCl + KCL), at $\eta_{NaCl} = 0.00$ (purple) and $\eta_{NaCl} = 0.21$ (black). Curves are calculated using model discussed in text. Symbols and error bars as in Figs. 2 and 3, except: unfilled for circles which represent calcite solubility in one and two-salt solutions calculated using Eqs. (7)-(9) and (23).
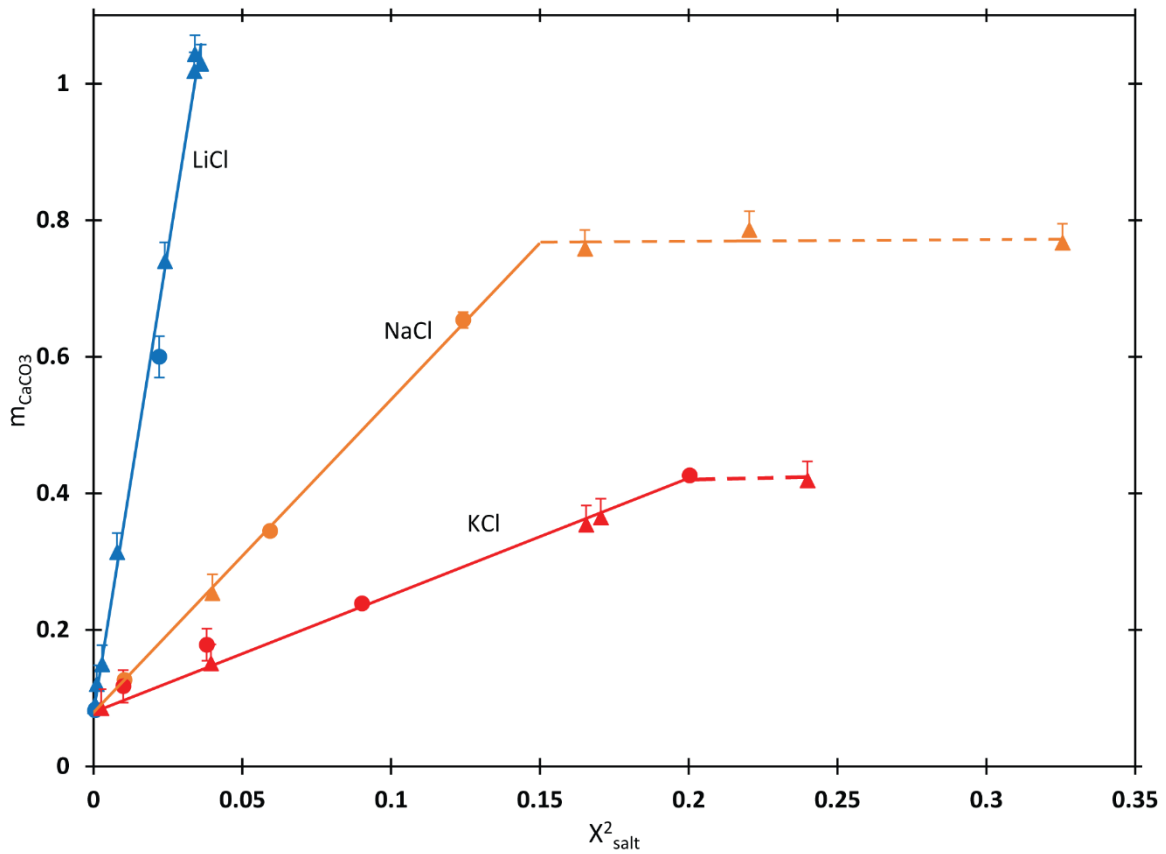
Figure 6. Calcite solubility (molality) vs. the square of total salt mole fraction. Lines represent linear regression of the salt-undersaturated data [Eqs. (7)-(9)], (see text). Symbols and error bars as in Figs. 2 and 3.
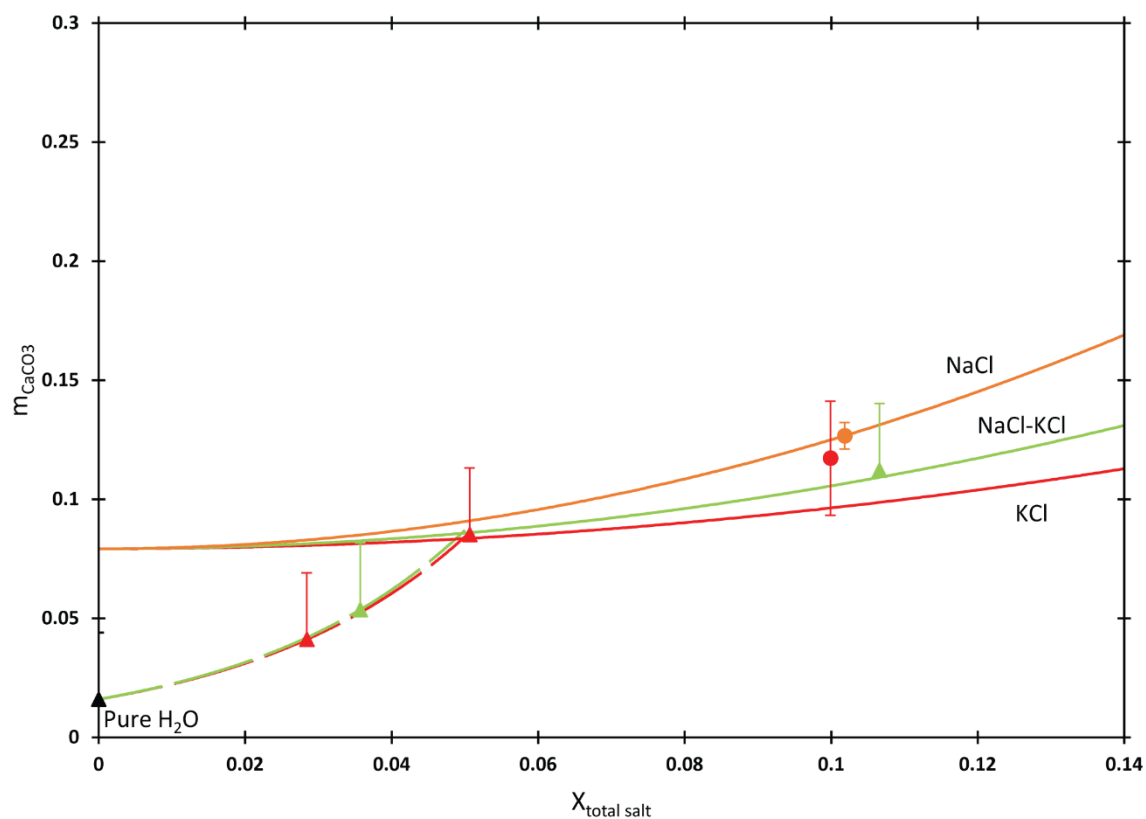
Figure 7. Calcite solubility (molality) vs. total salt mole fraction at low salt concentration. The data depart from the fitted curves at these conditions and trend towards calcite solubility in pure H_2O (shown as long-dashed lines). This change in behavior suggests the dominant species in solution may differ in low salt concentration solutions. Symbols and error bars as in Figs. 2 and 3; except for long-dashed lines.
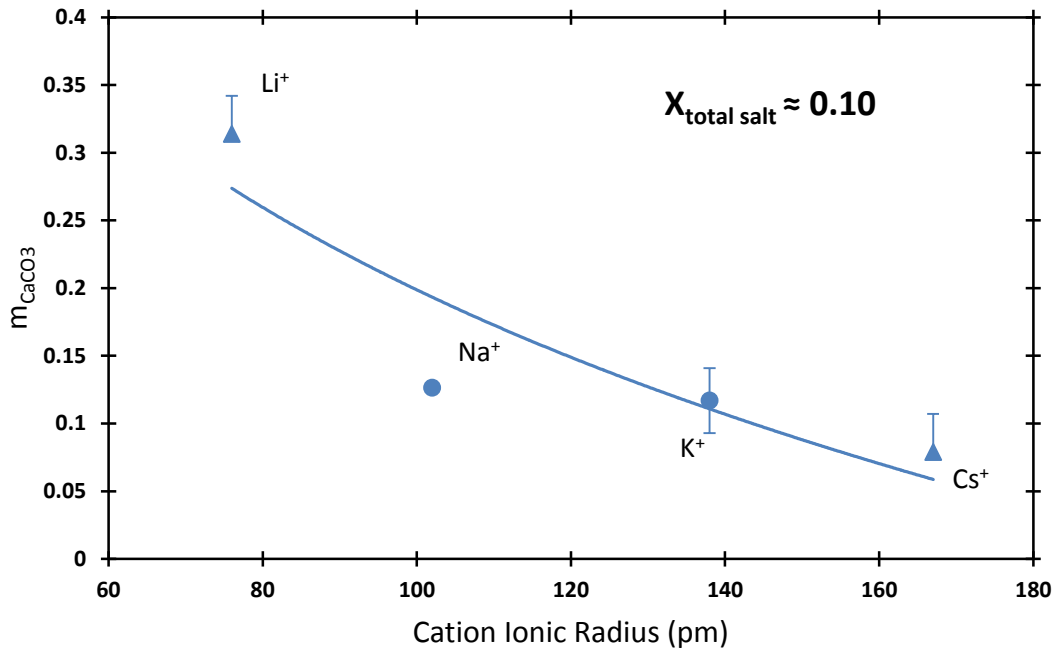
Figure 8. Calcite solubility (molality) vs. ionic radius of salt cation. All experiments at $X_{total\ salt} \approx$ 0.10. Experiments show trend of increasing calcite solubility with decreasing cation size. Symbols and error bars as in Fig. 2.
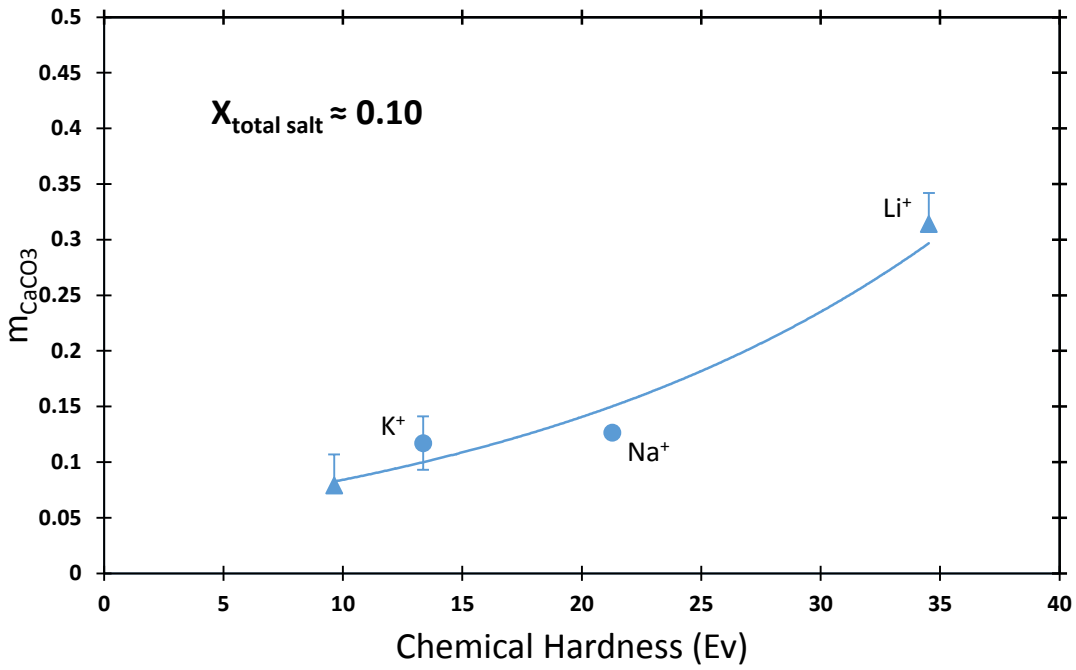
Figure 9. Calcite solubility (molality) vs. chemical hardness of salt cation. Chemical hardness calculated with Eq. (19) (see text). Data shows trend of increasing calcite solubility with increasing chemical hardness of salt cation. Symbols and error bars as in Fig. 2.
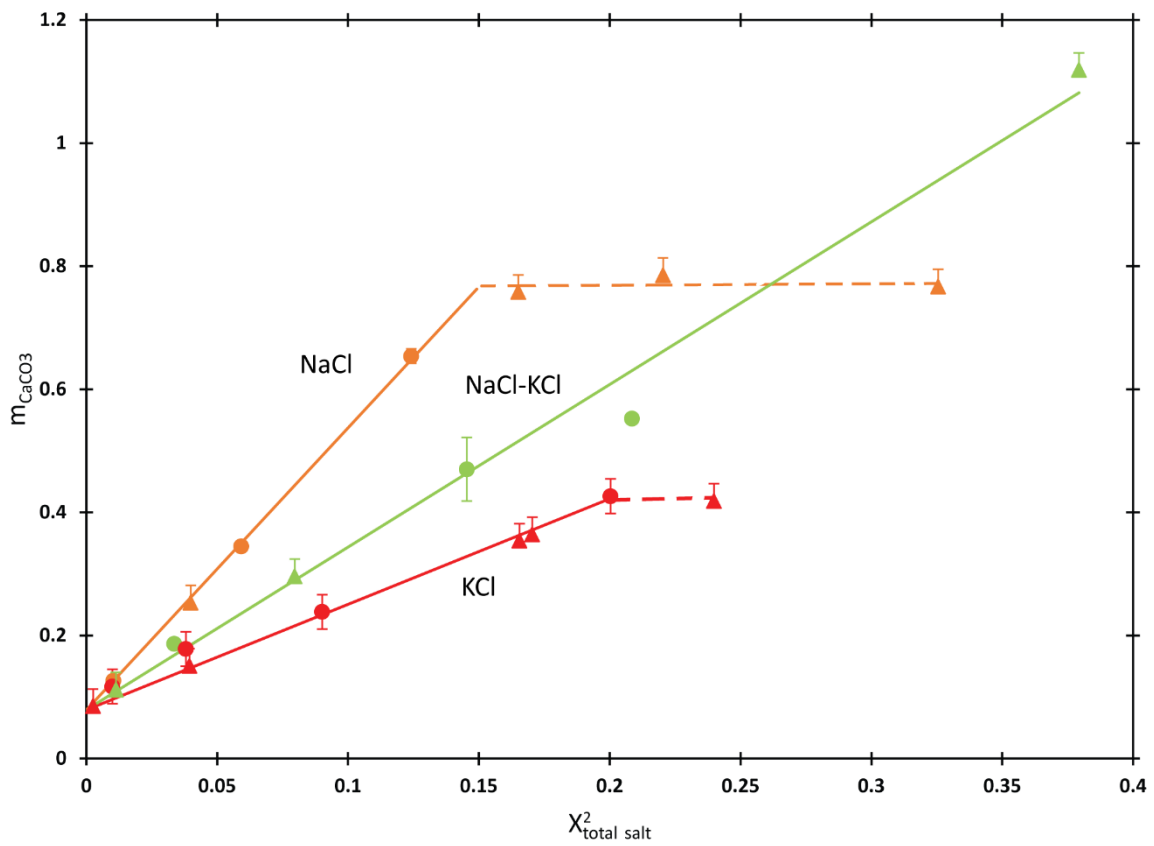
Figure 10. Calcite solubility (molality) vs. the square of total salt mole fraction. Note that the curve for 1:1 molar ratio mixture of NaCl and KCl is not halfway between the curves for pure NaCl and KCl. Symbols and error bars as in Figs. 2 and 3.

48
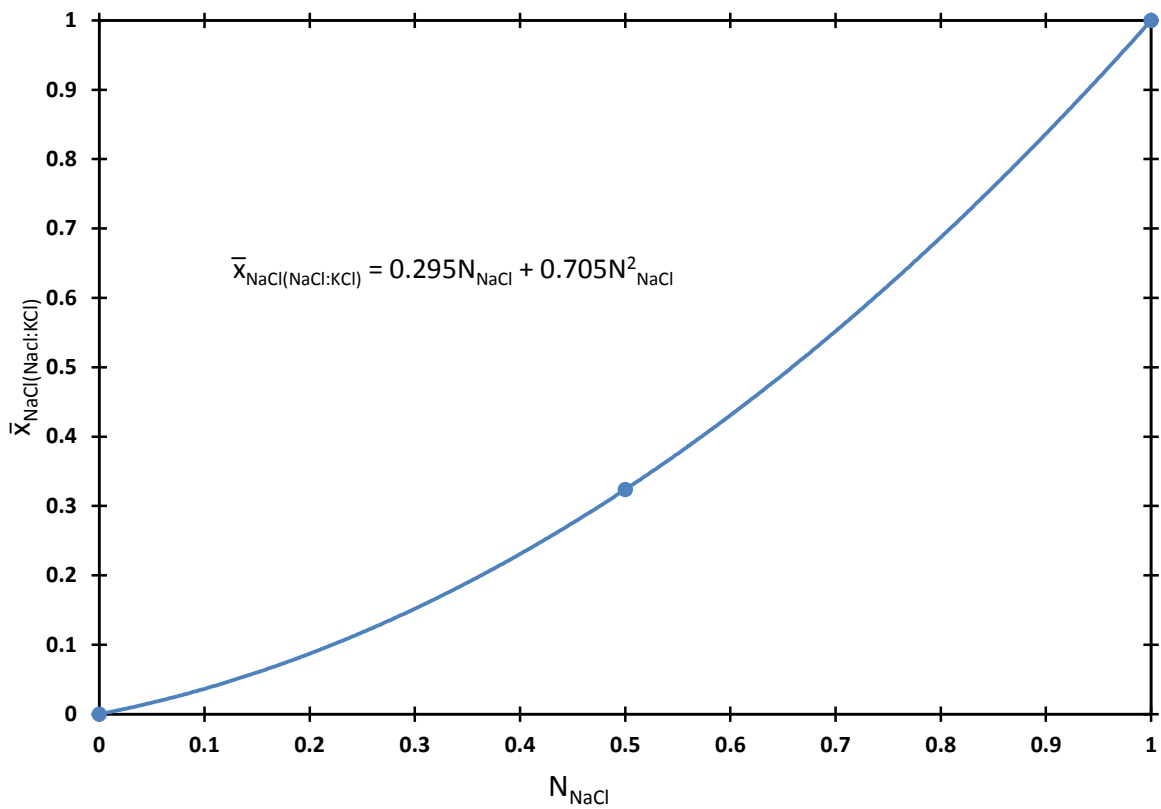
Figure 11. Variation in $\overline{x}_{NaCl(NaCl:KCl)}$ with N_{NaCl} in NaCl-KCl solutions. Fitted second order polynomials of the type shown were used to derive $\overline{x}_{i(A:B)}$ for all two-salt solutions (see text).
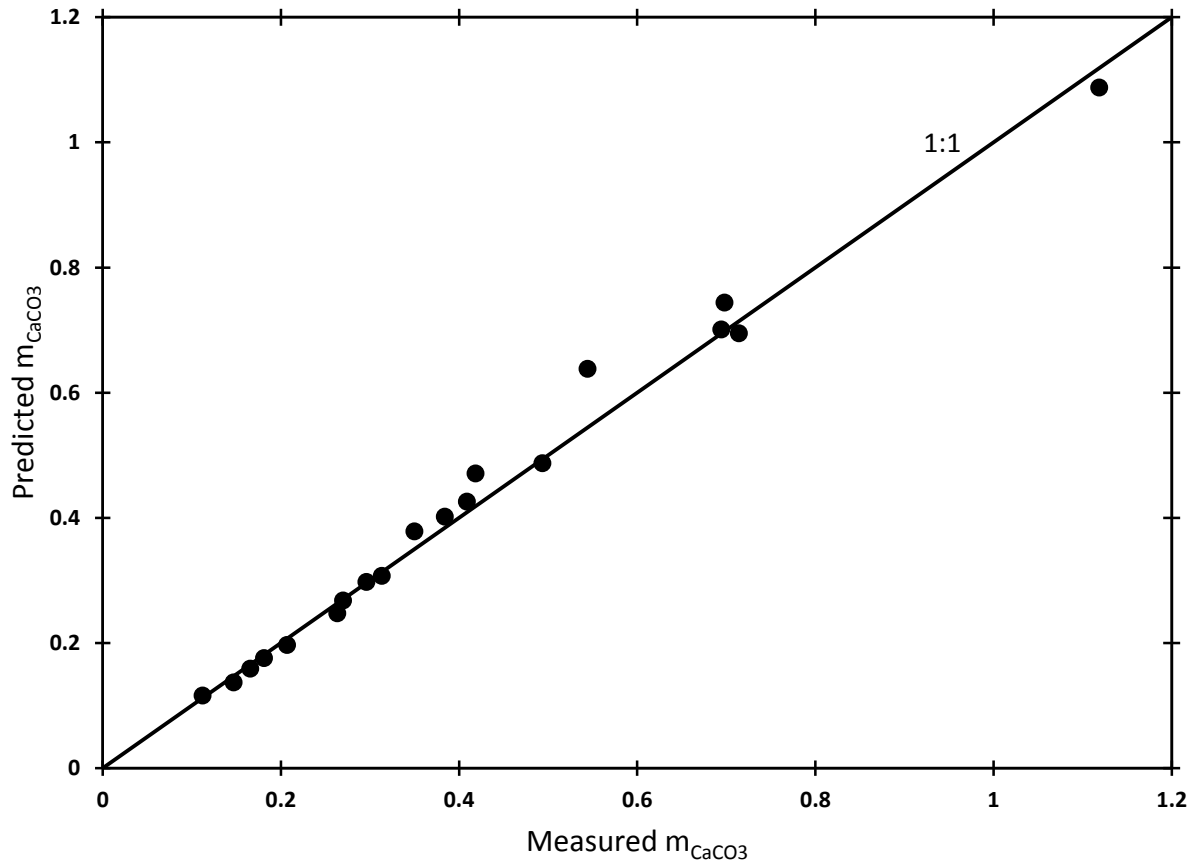
Figure 12. Predicted calcite solubility vs. measured calcite solubility in two-salt solutions. Predicted calcite solubility calculated from values of $\overline{x}_i$ and Eq. (23) (see text). Data plot along a 1:1 line, demonstrating that Eq. (23) accurately predicts calcite solubility in mixed-salt solutions, with an average deviation of 6.14%.
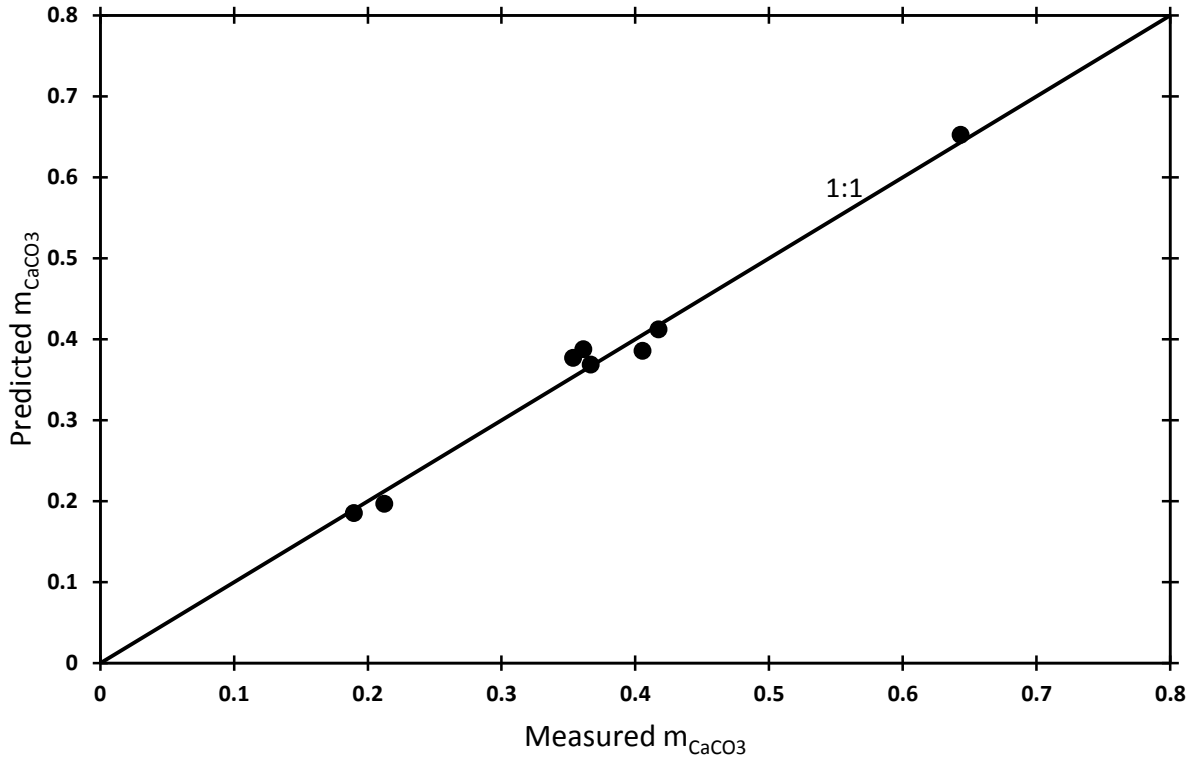
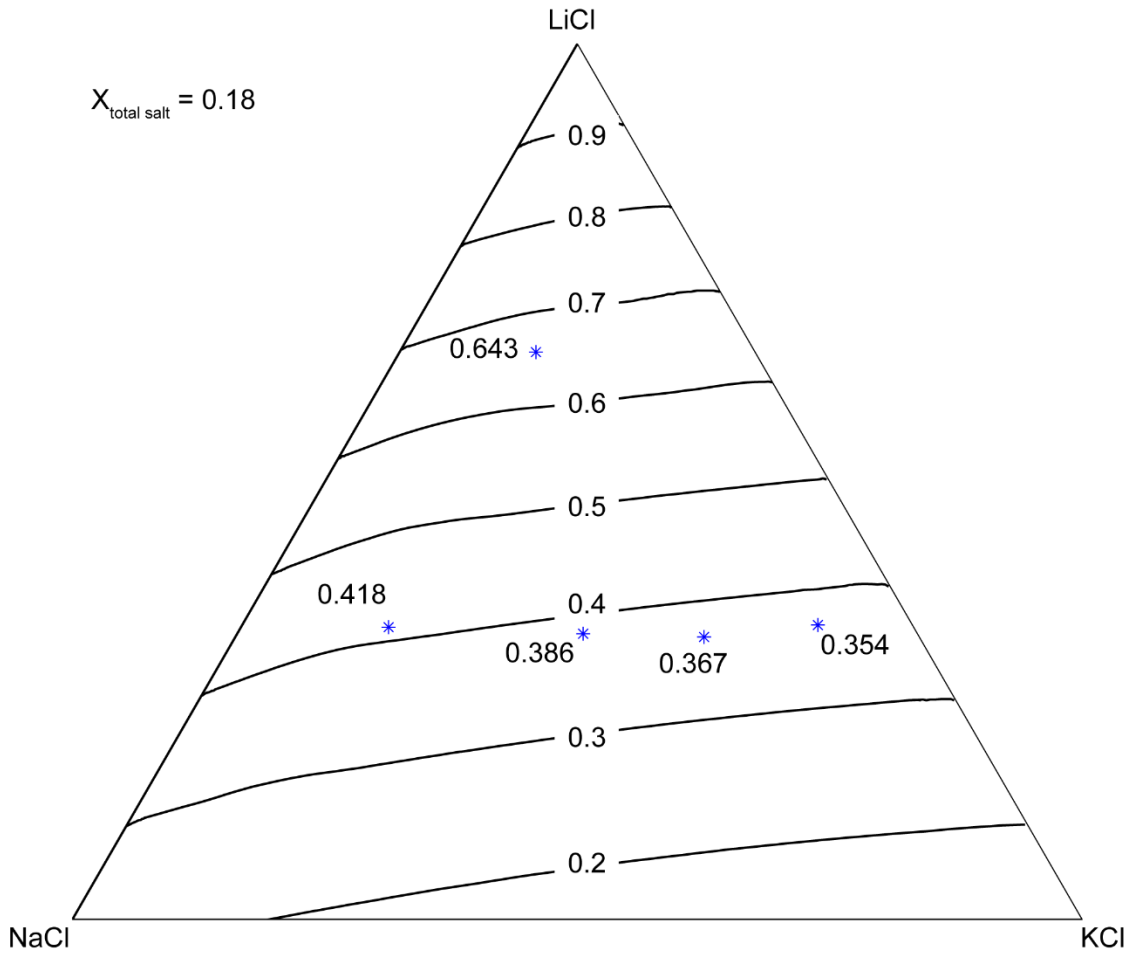**Figure 13**. Predicted calcite solubility vs. measured calcite solubility in three-salt solutions. Predicted calcite solubility calculated using $\overline{x}_i$ and Eq. (30) (see text). Data plot along a 1:1 line, demonstrating that Eq. (30) accurately predicts calcite solubility in three-salt solutions, with an average percent deviation of 1.32%.
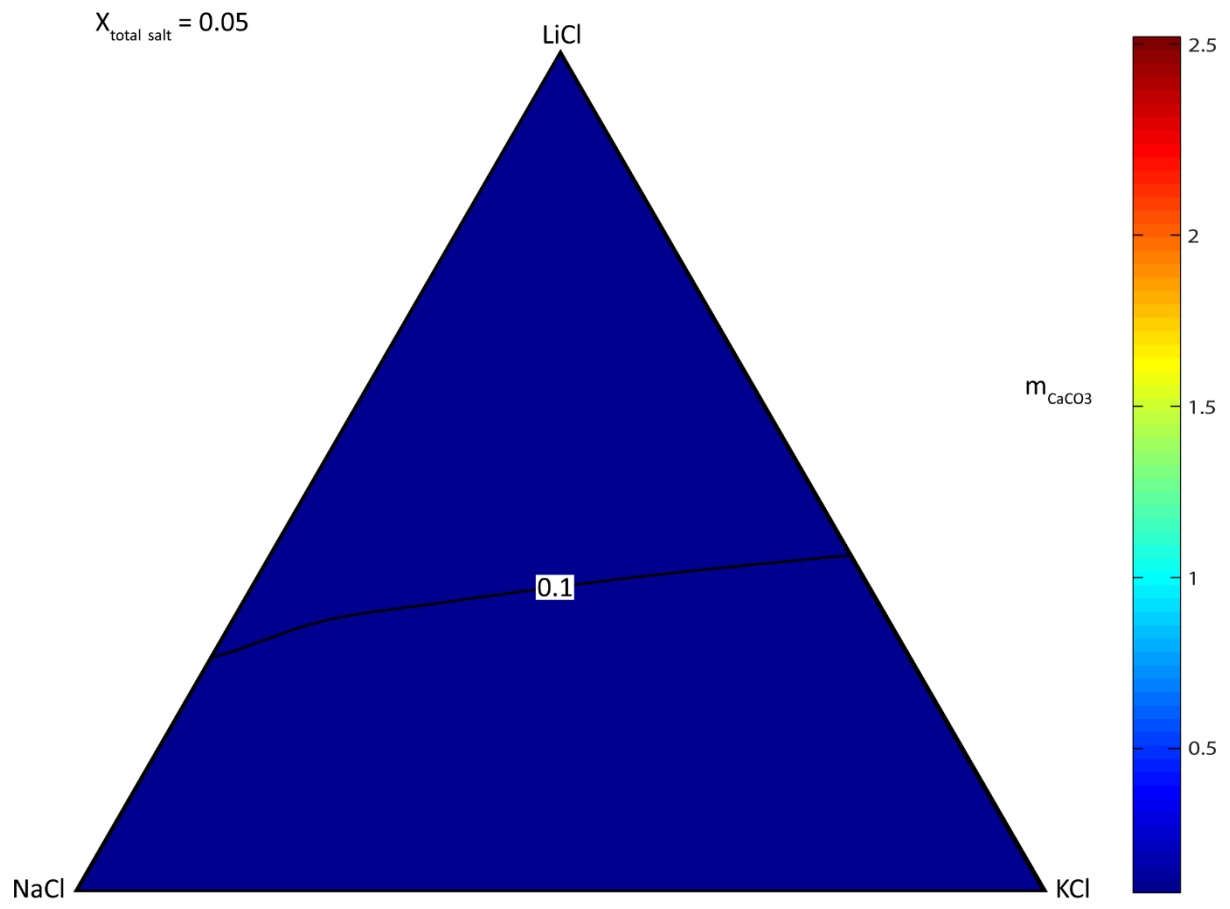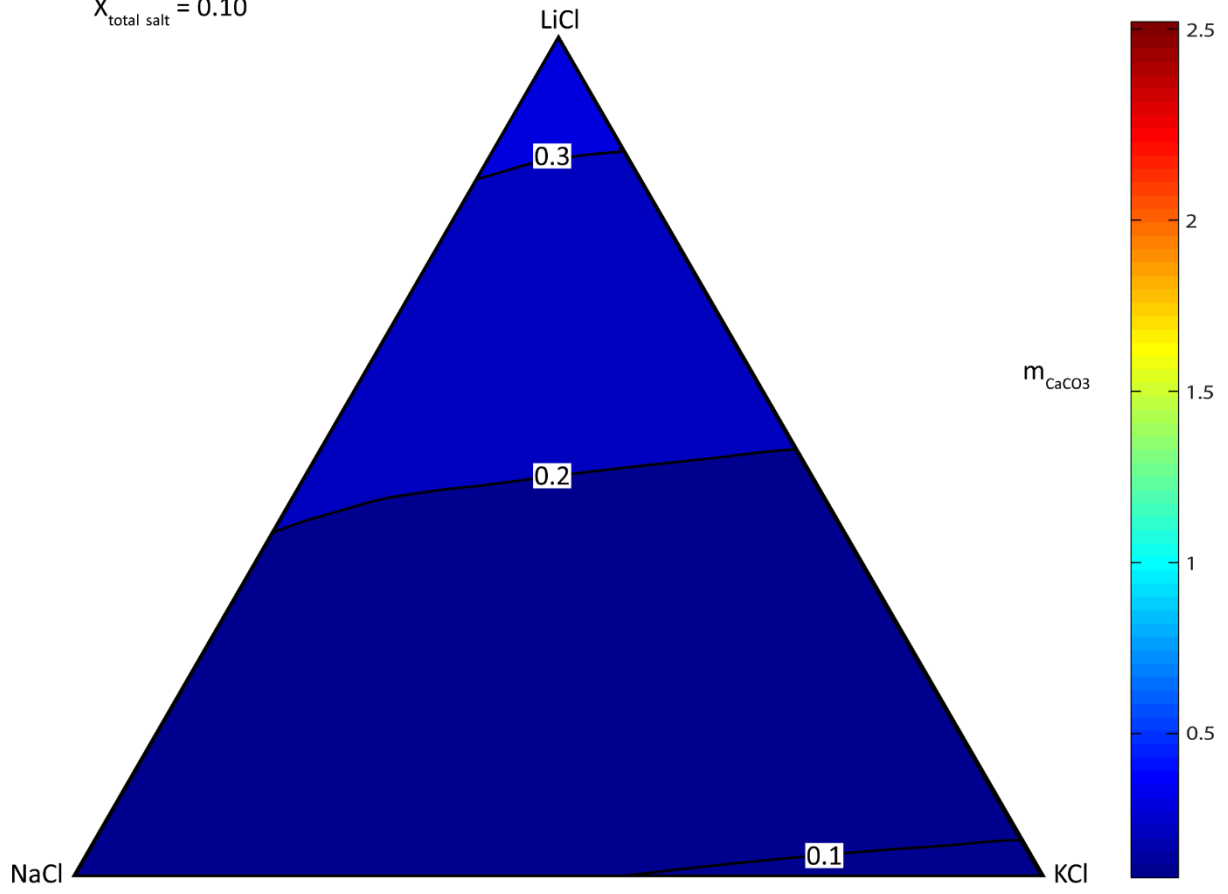
Figure 14. Ternary diagram with contours of constant calcite solubility (molality) at total salt mole fraction = 0.18, predicted using $\bar{x}$ and Eq. (30) (see text). Points are experiments labeled with measured calcite solubility.
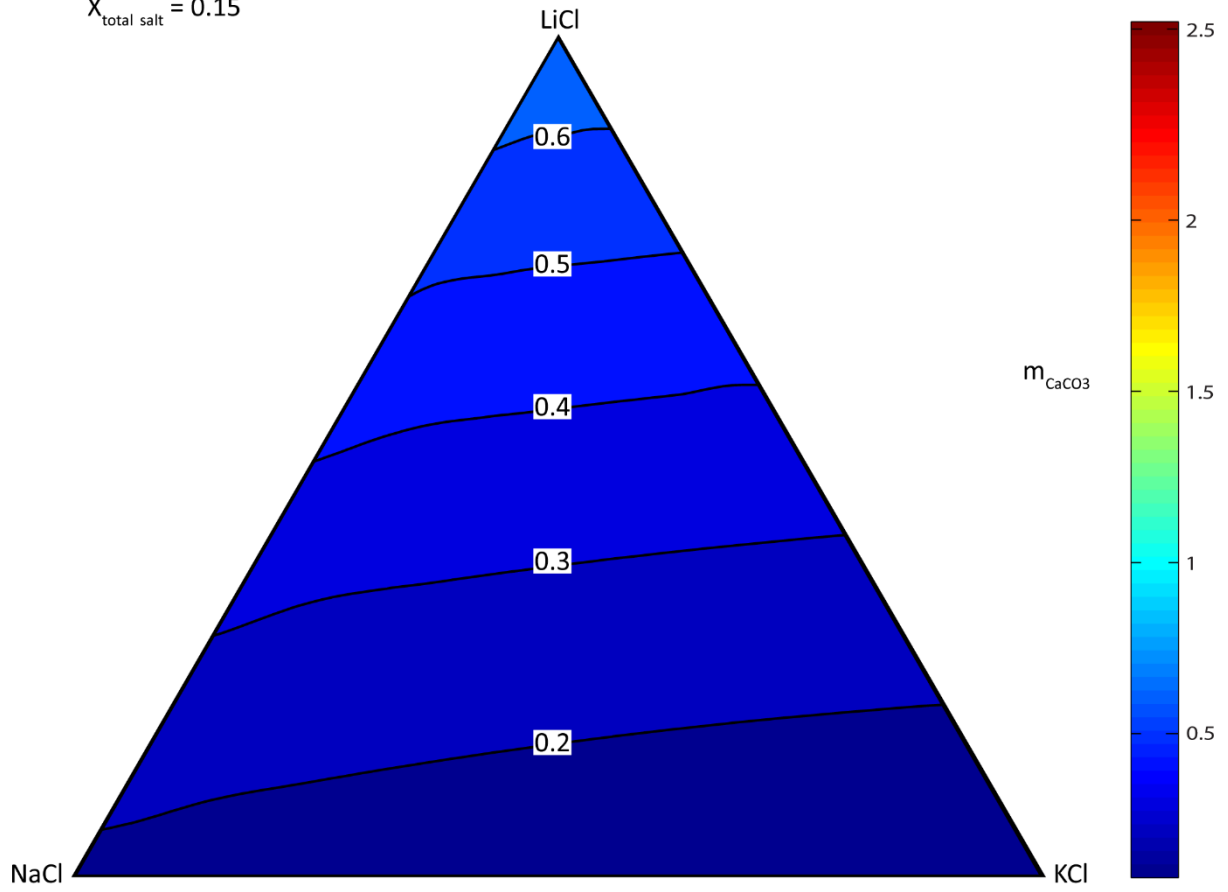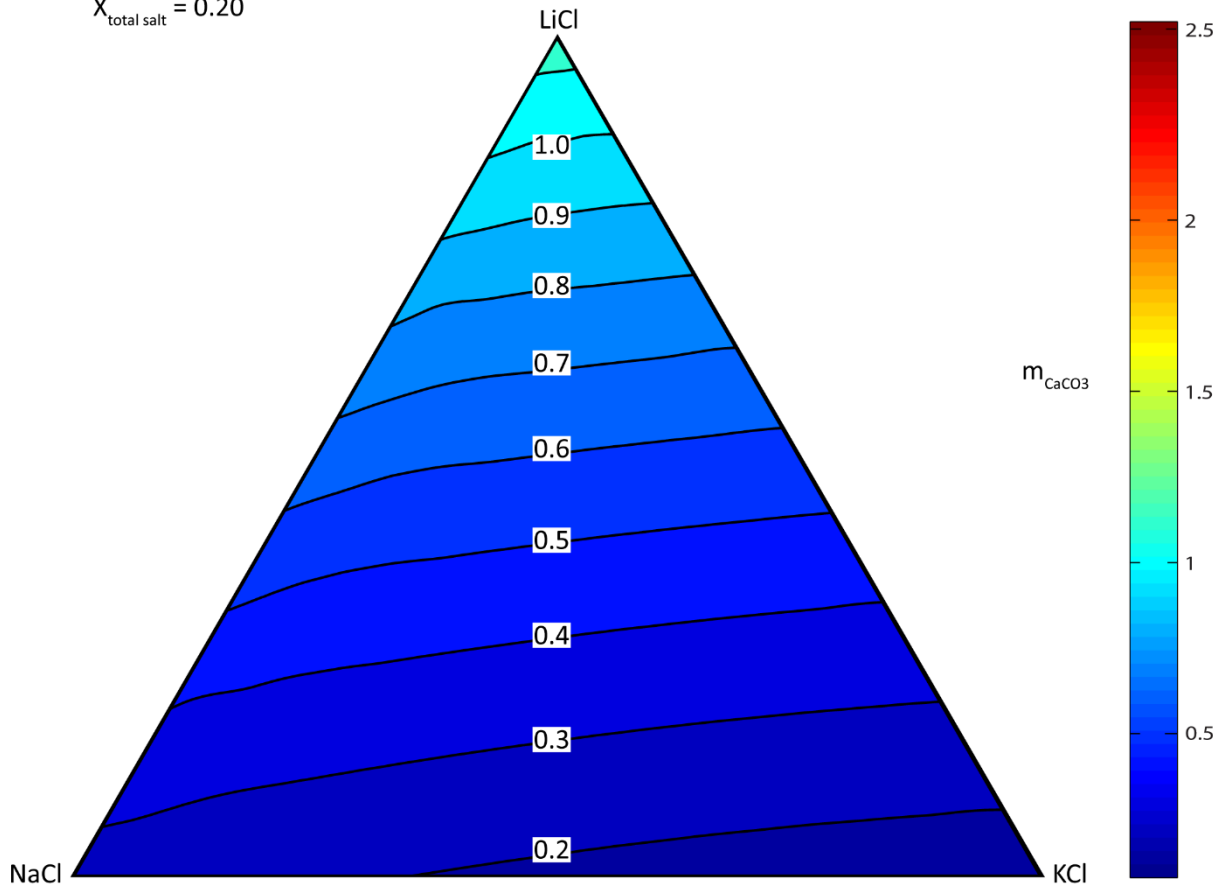
A

B

C

$X_{total\ salt} = 0.15$

LiCl

0.6

0.5

0.4

0.3

0.2

NaCl

KCl

m_{CaCO3}

2.5

2

1.5

1

0.5

D

E

X$_{total\ salt}$ = 0.25
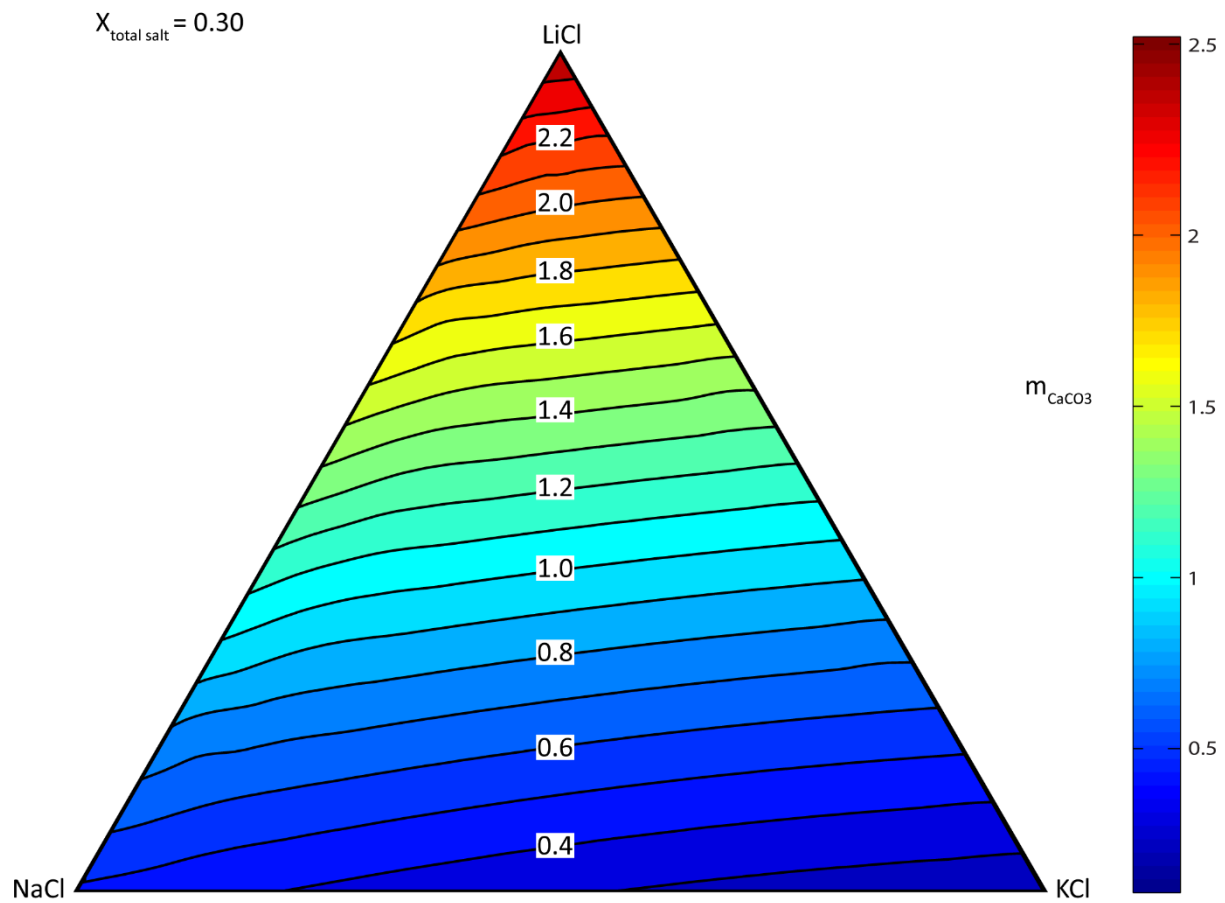
LiCl

NaCl

KCl

m$_{CaCO3}$
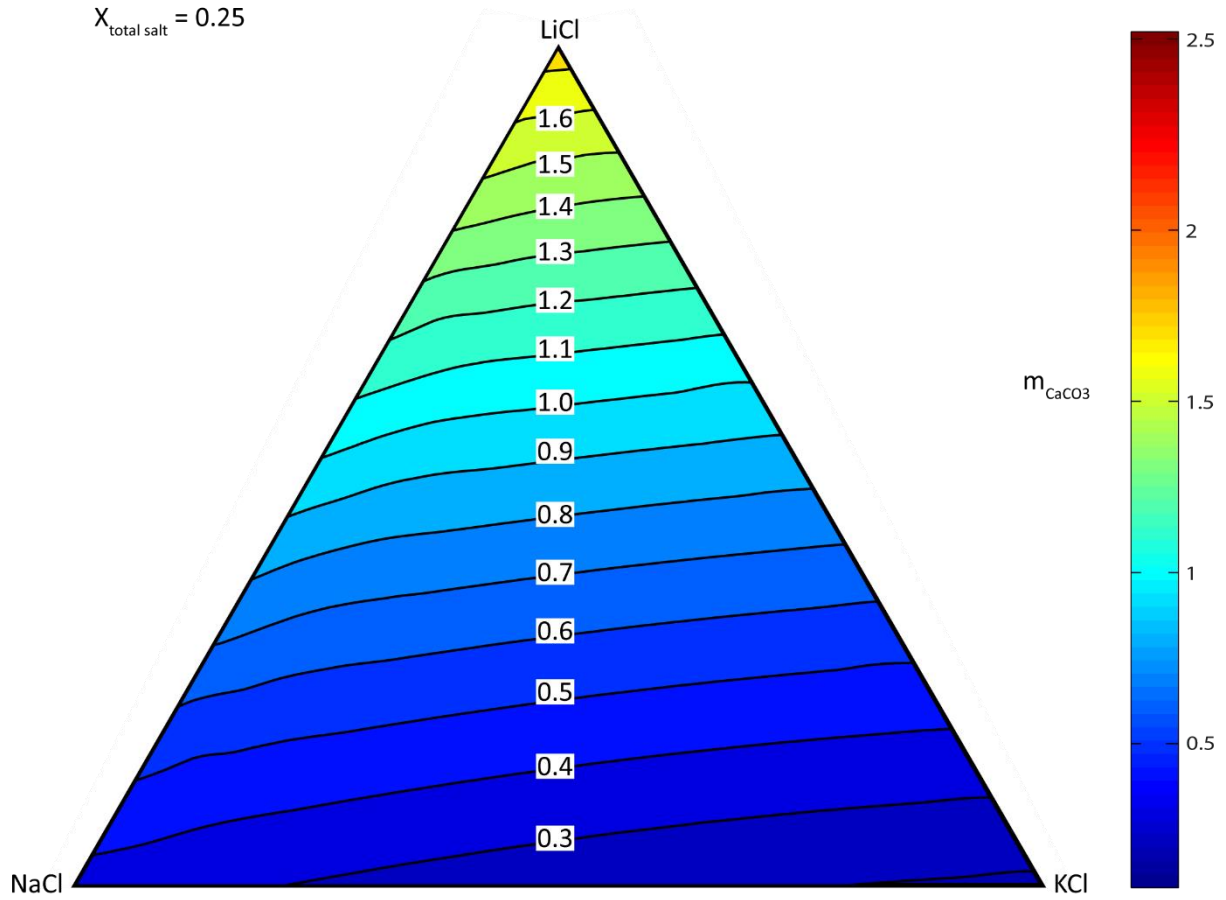
F

Figure 18. Ternary diagrams with contours of constant calcite solubility (molality), calculated using $\overline{x}$ and Eq. (30) (see text). All figures use the same contour interval and color scale. Figures A-F are ordered with increasing total salt mole fraction.

REFERENCES

Ague, J. J., & Nicolescu, S. (2014). Carbon dioxide released from subduction zones by fluid-mediated reactions, *7*(May), 1–6.

Alt, J., & Teagle, D. (1999). The uptake of carbon during alteration of ocean crust. *Geochimica et Cosmochimica Acta*, *63*(10), 1527–1535.

Aranovich, L. Y., & Newton, R. C. (1996). H 2 O activity in concentrated NaCl solutions at high pressures and temperatures measured by the brucite-periclase equilibrium. *Contributions to Mineralogy and Petrology*, *125*(2-3), 200–212.

Aranovich, L. Y., & Newton, R. C. (1997). H 2 O activity in concentrated KCl and KCl-NaCl solutions at high temperatures and pressures measured by the brucite-periclase equilibrium. *Contributions to Mineralogy and Petrology*, *127*(3), 261–271.

Baratov, R. B., Gnutenko, N. A., & Kuzemko, V.N. (1984). Regional carbonization connected with the epi-hercynian tectogenesis in the souther Tien Shan. *Doklady Akademiia Nauk S. S. R.*, 274, 124-126.

Blundy, J., Cashman, K. V., Rust, A., & Witham, F. (2010). A case for CO2-rich arc magmas. *Earth and Planetary Science Letters*, *290*(3-4), 289–301.

Bohlen, S. R. (1984). Equilibria for precise pressure calibration and a frictionless furnace assembly for the piston-cylinder apparatus. *Neues Jahrb Miner Moatsh*, 9, 404-412.

Bouilhol, P., Burg, J.-P., Bodinier, J.-L., Schmidt, M. W., Bernasconi, S. M., & Dawood, H. (2012). Gem Olivine and Calcite Mineralization Precipitated From Subduction-Derived Fluids in the Kohistan Arc-Mantle (Pakistan). *The Canadian Mineralogist*, *50*(5), 1291–1304.

Caciagli, N.C. (2001). The solubility of calcite in in water at 5-16 kilobars and 500-800°C. M.Sc. Thesis, University of California, Los Angeles.

Caciagli, N. C., & Manning, C. E. (2003). The solubility of calcite in water at 6-16 kbar and 500-800 C. *Contributions to Mineralogy and Petrology*, *146*(3), 275–285.

Dahlgren, S., & Bogoch, R. (1993). Hydrothermal dolomite marbles associated with charnockitic magmatism in the Proterozoic Bamble Shear Belt, south Norway. *Contributions to Mineralogy and Petrology*, *993*, 394–409.

Dasgupta, R. (2013). Ingassing, Storage, and Outgassing of Terrestrial Carbon through Geologic Time. *Reviews in Mineralogy and Geochemistry*, *75*(1), 183–229.

Dasgupta, R., & Hirschmann, M. M. (2010). The deep carbon cycle and melting in Earth's interior. *Earth and Planetary Science Letters*, *298*(1-2), 1–13.

Duncan, M. S., & Dasgupta, R. (2014). CO2 solubility and speciation in rhyolitic sediment partial melts at 1.5–3.0GPa – Implications for carbon flux in subduction zones. *Geochimica et Cosmochimica Acta*, *124*, 328–347.

Fein, J. B., & Walther, J. V. (1989). Calcite solubility and speciation in supercritical NaCI-HCI aqueous fluids, 317–324.

Frezzotti, M. L., Selverstone, J., Sharp, Z. D., & Compagnoni, R. (2011). Carbonate dissolution during subduction revealed by diamond-bearing rocks from the Alps. *Nature Geoscience*, *4*(10), 703–706.

Fu, B., Touret, J., & Zheng, Y. (2001). Fluid inclusions in coesite-bearing eclogites and jadeite quartzite at Shuanghe, Dabie Shan (China). *Journal of Metamorphic Geology*, (1983).

Kerrick, D. M., & Connolly, J. a. (2001). Metamorphic devolatilization of subducted marine sediments and the transport of volatiles into the Earth's mantle. *Nature*, *411*(6835), 293–6.

Manning, C. E., & Boettcher, S. L. (1994). Rapid-quench hydrothermal experiments at mantle pressures and temperatures, *79*, 1153–1158.

Manning, C. E., & Ingebritsen, S. (1999). Permeability of the continental crust: Implications of geothermal data and metamorphic systems. *Reviews of Geophysics*, (1998), 127–150.

Manning, C.E., & Aranovich, L. Y. (in review) Brines at High Pressure and Temperature: Thermodynamic, Petrologic, and Geochemical Effects.

Marschall, H. R., & Schumacher, J. C. (2012). Arc magmas sourced from mélange diapirs in subduction zones. *Nature Geoscience*, *5*(12), 862–867.

Nehring, F., Foley, S.F., Holtta, P., & Van Den Kerkhof, A.M. (2009). Internal Differentiation of the Archean Continental Crust: Fluid-Controlled Partial Melting of Granulites and TTG-Amphibolite Associations in Central Finland. *Journal of Petrology*, 50, 3-35.

Newton, R. C., Aranovich, L. Y., Hansen, E. C., & Vandenheuvel, B. A. (1998). Hypersaline fluids in Precambrian deep-crustal metamorphism. *Precambrian Research*, 91, 41-63.

Newton, R. C., & Manning, C. E. (2002). Experimental determination of calcite solubility in H2O-NaCl solutions at deep crust/upper mantle pressures and temperatures: Implications for metasomatic processes. *American Mineralogist*, *87*, 1401–1409.

Newton, R. C., & Manning, C. E. (2010). Role of saline fluids in deep-crustal and upper-mantle metasomatism: insights from experimental studies. *Geofluids*, 10, 58-72.

Oliver, N., & Cartwright, I. (1993). The stable isotope signature of kilometre-scale fracturedominated metamorphic fluid pathways, Mary Kathleen, Australia. *Journal of Metamorphic Petrology*, 705–720.

Parr, R. G., & Pearson, R. G. (1983). Absolute hardness: companion parameter to absolute electronegativity. *Journal of the American Chemical Society*, *105*(26), 7512–7516.

Phillipot, P., & Selverstone, J. (1991). Trace-element-rich brines in eclogitic veins: implications for fluid composition and transport during subduction. *Contributions to Mineralogy and Petrology*, 106, 417-430.

Plank, T., & Langmuir, C. H. (1998). The chemical composition of subducting sediment and its consequences for the crust and mantle. *Chemical Geology*, *145*(3-4), 325–394.

Scott, A. F., (1932). The apparent volumes of salts in solutions III. Saturated solutions of mixed electrolytes. *The Journal of Physical Chemistry*, 36(3), 1022-1034.

Shmulovich, K. I., Yardley, B. W. D., & Graham, C. M. (2006). Solubility of quartz in crustal fluids: experiments and general equations for salt solutions and H2O-CO2 mixtures at 400-800 °C and 0.1-0.9 GPa. *Geofluids*, *6*(2), 154–167.

Shannon, R. D. (1976). Revised effective ionic radii and systematic studies of interatomic distances in halides and chalcogenides. *Acta Crystallographica,* 32, 751-767.

Royal Society, & U.S. National Academy of Sciences (2014). Climate Change Evidence & Causes. *The National Academies Press*.

Van den Berg, R., & Huizenga, J. (2001). Fluids in granulites of the Southern Marginal Zone of the Limpopo belt, South Africa. *Contributions to Mineralogy and Petrology,* 141, 529-545.

Wickham, S. M., Janardhan, A. S., & Stern, R. J. (1994). Regional Carbonate Alteration of the Crust by Mantle-Derived Magmatic Fluids , Tamil Nadu , South India. *The Journal of Geology, 102*(4), 379–398.

Xiao, Y.L., Hoefs, J., Van Den Kerkhof, A.M., & Li, S.G. (2001). Geochemical constraints of the eclogite and granulite facies metamorphism as recognized in the Raobazhai complex from North Dabie Shan, China. *Journal of Metamorphic Geology,* 19, 3-19.

Yardley, B. W. D., & Graham, J. T. (2002). The origins of salinity in metamorphic fluids. *Geofluids*, *2*(4), 249–256.